Global Biogeochemical Cycles

RESEARCH ARTICLE
10.1029/2022GB007453

# Particulate Trace Metal Sources, Cycling, and Distributions on the Southwest African Shelf

**Ali A. Al-Hashem[1,2], Aaron J. Beck[1], Stephan Krisch[1,3], Jan-Lukas Menzel Barraqueta[1,4], Tim Steffens[1], and Eric P. Achterberg[1,2]**

[1]GEOMAR Helmholtz Centre for Ocean Research Kiel, Kiel, Germany, [2]Christian-Albrechts-University of Kiel, Kiel, Germany, [3]Now at Bundesanstalt für Gewässerkunde, Koblenz, Germany, [4]Now at European Ecological Consulting S.L. (EECO), Amorebieta, Spain

**Key Points:**

- Different oxidation kinetics lead to decoupled Fe and Mn oxide redox cycling within oxygen-depleted waters on the Benguela Shelf
- Lower lability of particulate phosphorus (~41%) indicate potential refractory biogenic source on Benguela shelf
- Nepheloid particles formed important sources of Fe and Mn oxides that adsorb trace metals (TMs), and serve as potential TM sources from shelf to open ocean

**Supporting Information:**

Supporting Information may be found in the online version of this article.

**Correspondence to:**

A. A. Al-Hashem,
aalhashem@geomar.de

**Citation:**

Al-Hashem, A. A., Beck, A. J., Krisch, S., Menzel Barraqueta, J.-L., Steffens, T., & Achterberg, E. P. (2022). Particulate trace metal sources, cycling, and distributions on the southwest African shelf. *Global Biogeochemical Cycles*, *36*, e2022GB007453. https://doi.org/10.1029/2022GB007453

Received 13 MAY 2022
Accepted 2 NOV 2022



**Abstract** We present labile (L-pTM) and refractory (R-pTM) particulate trace metal distributions of Fe, Mn, Al, Ti, Co, Zn, Cd, Ni, Pb, Cu, and P for a transect along the southwest African shelf and an off-shore section at 3°S of the GEOTRACES GA08 section cruise. Particle sources and biogeochemical cycling processes are inferred using particle-type proxies and elemental ratios. Enhanced concentrations of bio-essential L-pTMs (Zn, Cu, Ni, Cd, Co, and P) were observed in the Benguela upwelling region, attributed to enhanced primary production. Bio-essential pTM stoichiometric ratios (normalized to pP) were consistent with phytoplankton biomass across the transect, except for Fe and Mn, which included adsorbed and labile oxide phases. Low pP lability (~41%) suggests a potential refractory biogenic source on the Benguela shelf. Variable labilities observed between stations along the transect indicated potentially different biogenic pP labilities among different plankton groups. Benthic resuspension was prevalent in (near-)bottom waters along the transect and formed an important source of Fe and Mn oxides. Lithogenic particles along the entire shelf were Mn deficient and particles on the Benguela shelf were enriched in Fe, consistent with regional sediment compositions. Enhanced available-Fe (dissolved + labile particulate Fe) concentrations (up to 39.6 nM) were observed in oxygen-deficient (near-)bottom waters of the Benguela shelf coinciding with low L-pMn. This was attributed to the faster oxidation kinetics of Fe, allowing Fe-oxide precipitation and retention on the shelf, while Mn oxidation was slower. Enhanced L-pFe in the Congo River plume, which comprised as much as 93% of the available-Fe pool, was attributed to increased scavenging and formation of Fe oxides. Increased scavenging of other particle-reactive trace metals (TMs) (Mn, Al, and Pb) was also apparent in Congo-influenced waters. However, particles did not play a significant role in transporting TMs off-shelf within Congo plume waters.

**Plain Language Summary** Trace metals (TMs) are important to the functioning of marine ecosystems, with a range of TMs required as micronutrients by phytoplankton, while some are contaminants, and others may serve as tracers of water masses. Marine particles are key to the biogeochemical cycling of most TMs as sources, sinks, and essential transport vectors in the ocean. The transport and fate of TMs are often multi-faceted and upon a multitude of inter-related factors including particle sources/types, and environmental conditions, many of which are directly evident on continental shelves. Continental shelves thus are important conduits through which TMs are transferred from land to the ocean. Despite their importance, shelves are still understudied with respect to trace metal cycling. Here we present data from the longest continental shelf transect for TMs to date, which traversed through several key biogeochemical regimes, including an oxygen depleted zone, upwelling region, and a river plume, providing unique gradients under which particles from various sources and internal cycling processes were studied. A chemical leach was applied to marine particles to differentiate between particle types and phases. Utilizing the contrasting marine environments and particle types encountered along the transect, we highlight the major biogeochemical cycling dynamics controlling trace metal distributions, which provide valuable regional insights which may be extended to other regions of the global ocean.

## 1. Introduction

Trace metals (TMs) are important to the functioning of marine ecosystems, with a range of TMs required as micronutrients by phytoplankton and serving as essential cofactors in metalloenzymes (Sunda, 1989, 2012). Iron (Fe), cobalt (Co), and manganese (Mn) are potentially (co-)limiting oceanic primary production (Browning et al., 2017, 2021; Martin et al., 1989; Moore et al., 2013) and, therefore their supply, removal and retention

processes in the water column are important controls on phytoplankton growth. Marine particles play a vital role in the marine biogeochemical cycling of TMs as essential transport vectors (Jeandel et al., 2015), acting as sources and sinks of dissolved TMs (dTMs) through adsorption (e.g., Fe, Mn, Co, lead (Pb), copper (Cu), and aluminum (Al)), precipitation/dissolution (e.g., Fe and Mn), and/or bio-assimilation and remineralization (e.g., Fe, Mn, Zn, Cu, nickel (Ni), Co, cadmium (Cd)) (Boyd et al., 2017; Bruland & Lohan, 2003; Bruland et al., 2014; Goldberg, 1954; Morel & Price, 2003; Turekian, 1977). The interactions and exchanges between solid and dissolved TM phases are multi-faceted, relying upon interrelated biogeochemical mechanisms controlled by particle sources (types), characteristics, and environmental conditions (Anderson, 2020; Boyd et al., 2017; Bruland & Lohan, 2003; Bruland et al., 2014; Jeandel et al., 2015) many of which are evident on continental shelves (Elrod et al., 2004). Continental shelves form an important conduit for transfer between land and ocean of marine particles, yet remain understudied across large ocean basins (Charette et al., 2016; Henderson & Marchal, 2015).

The TM composition of marine particles reflects both particle source and biogeochemical cycling processes in the water column. Additional information about readily exchangeable or potentially soluble particulate TM (pTM) fractions can be gained by separating labile (L-pTM) from refractory particulate (R-pTM) phases. Elemental proxies are often employed as effective particle type indicators, namely particulate phosphorus (P) as a biogenic particle indicator, and an abundant lithogenic element (typically Al or Ti) for lithogenic particles (e.g., Lam, Ohnemus, et al., 2015; Lam, Twining, et al., 2015; Lam et al., 2018; Lee et al., 2018; Liao & Ho, 2018; Martin et al., 1989; Ohnemus & Lam, 2015; Xiang & Lam, 2020). A chemical leaching application developed by Berger et al. (2008) (see Section 2.2) to access the labile phase is now widely adopted for the study of marine particles (Cutter et al., 2017). The labile particulate phase reflects the potentially bio-accessible, "exchangeable" pTM pool, which includes readily reduceable, surface-bound (adsorbed/scavenged), and intra-cellular TMs associated with biogenic particles, and authigenic particulate phases (i.e., Fe and Mn oxy-hydroxides) while leaving lithogenic and other refractory particle phases largely intact (Berger et al., 2008; Rauschenberg & Twining, 2015). Dissolved TM phases are often considered as the most reactive and bio-available to phytoplankton (Wells et al., 1995), but the L-pTM pool, particularly of Fe, comprises a significant fraction of the potentially available TM pool, and may buffer dissolved concentrations (e.g., Achterberg et al., 2018; Berger et al., 2008; Hurst & Bruland, 2008; Lippiatt, Brown, et al., 2010; Milne et al., 2017). Hence, the "available" TM pool inferred in this study is the sum of the dTM and L-pTM pools, consistent with the definition adopted elsewhere (namely, Berger et al., 2008; Birchill et al., 2017; Hurst et al., 2010; Lippiatt, Lohan, & Bruland, 2010; Milne et al., 2017; Twining et al., 2015).

The GEOTRACES GA08 section cruise, conducted in the southeast Atlantic Ocean, included the longest continental shelf transect sampled for TMs to date. The shelf transect traversed several major oceanographic features along the southwest African shelf, including the Benguela Upwelling System (BUS), an oxygen minimum zone (OMZ), and the Congo River plume. Regional particle sources included atmospheric deposition derived from surrounding deserts (Jickells, 2005; Prospero, 1996), riverine discharge (Vangriesheim et al., 2009), resuspended benthic sediment (Inthorn et al., 2006), and enhanced bio-assimilation of TMs into organic (biogenic) particles within the BUS (Carr, 2001; Shannon & Nelson, 1996). The combination of contrasting particle sources and oceanographic regimes that were sampled during the GA08 cruise offered unique gradients in pTM distributions under which TM biogeochemical cycling could be studied.

The primary goal of this study is to present, describe and interpret the pTM distributions and biogeochemical processes affecting pTMs along the southwest African shelf, and characterize dominant particle phases and sources of Fe, Zn, Cd, Mn, Co, Ni, Cu, Al, Ti, Pb, and P. The study was carried out utilizing chemically labile and refractory pTM phases, and elemental abundance ratios. We utilize dTM data and ancillary measurements from paired samples. Insights from our data set offered valuable insights to regional TM cycling processes, which may be extended to other shelf regions of the global ocean.

## 2. Materials and Methods

### 2.1. Study Region

This study focuses on samples collected along a southwest African coastal transect of the GA08 GEOTRACES section cruise, between 28.8°S and 3°S (Figure 1), conducted during the austral summer of 2015 (22 November–27 December) on *RV Meteor*. Regional water circulation includes the southward flowing Angola Current in the north

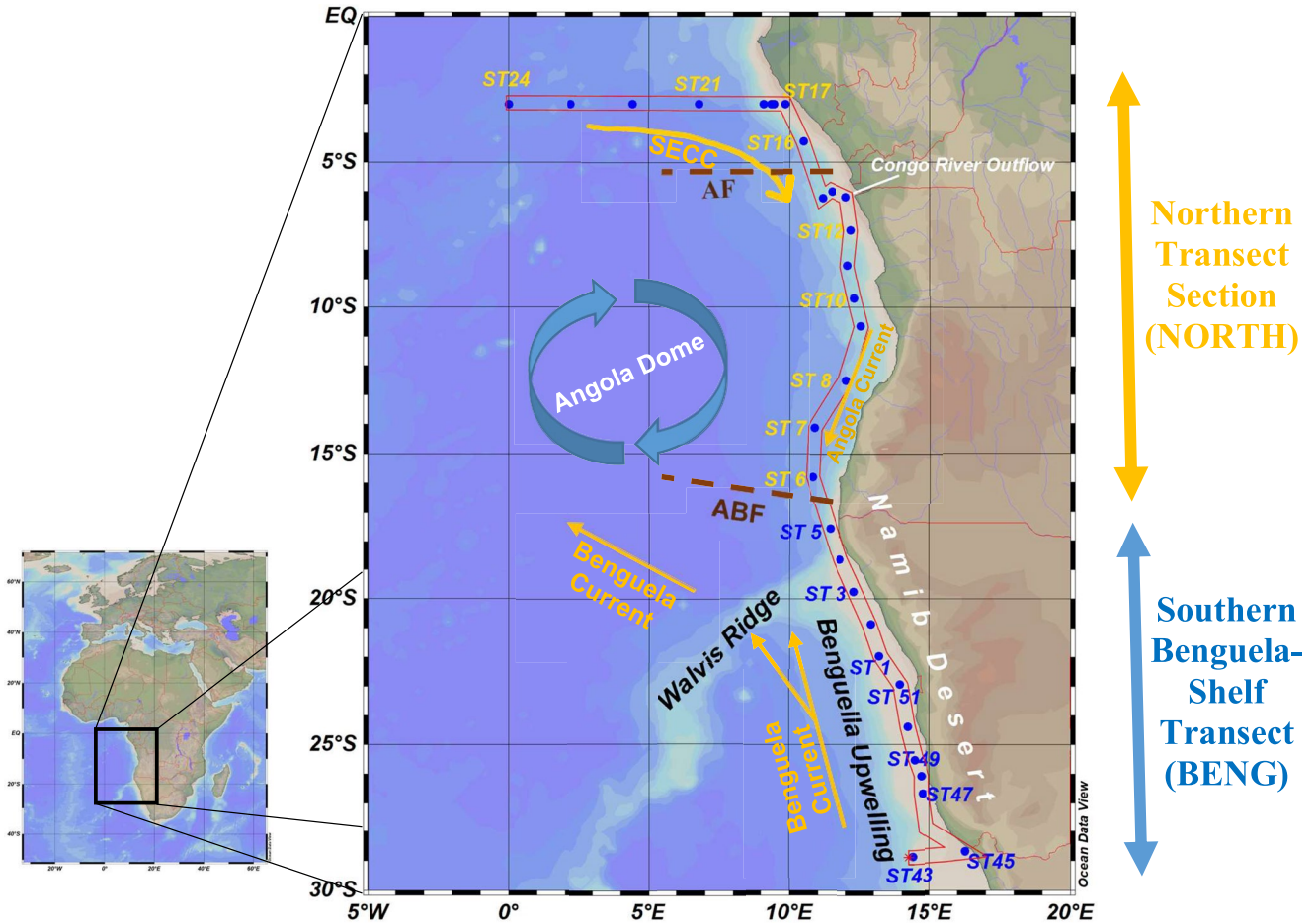


**Figure 1.** Map showing the large-scale circulation and oceanographic features that influence the Benguela ecosystem and Angola Basin, and part of the GA08 (M121) cruise track. Stations labeled in blue indicate the shallower stations above the Benguela shelf (BENG), and stations labeled in yellow indicate the Northern region stations (NORTH). ABF = Angola-Benguela Front; AF = Angola Front; SECC = South Equatorial Counter Current. Figure illustrations adapted from Shannon (2001).

bounded by the Tropical/Equatorial Eastern Atlantic Current, and the northward-flowing Benguela Current in the south bounded by the Agulhas current from the Indian Ocean (Peterson & Stramma, 1991; Shannon, 2001; Shannon & Nelson, 1996; Shannon et al., 1987). The two currents converge at the Angola-Benguela Front (ABF), north of Walvis Ridge, and are carried westward into the Angola Basin. The main water masses intersected along the transect are described below (see Section 3.1).

The transect extended from southern Namibia at the southernmost point (28.7°S) and across to the shelf waters at Gabon at the northernmost station (3°S), where a longitudinal transect away from the shelf to 0° Meridian was sampled. The seafloor depths of the stations along the transect varied between 53 and 4,501 m, including on-shelf and off-shelf stations. The cruise track traversed several oceanographic features along the shelf, including the Congo River outflow (stations [ST] 13–15; at 6.2°S), BUS (ST 43–51, 1–4; between 18.6°S and 28.8°S), and an OMZ that extended throughout the transect (at a depth of ~50–600 m), with more pronounced oxygen-depletion on the Benguela shelf (see Section 3.1). The Congo River provides a significant number of particles and organic matter to coastal waters (Vangriesheim et al., 2009), influencing TM cycling. Sampling nearest the Congo River outflow included a short (~100 km) transect of three stations (ST 13–15) at 6°S–6.2°S, approximately 40–140 km away from the Congo River mouth. Anoxic and sulfidic shelf sediments are documented within 50 km of some stations on the Benguela shelf (e.g., ST 51) (Borchers et al., 2005; Inthorn et al., 2006). Phosphorite deposits are also widely documented on the Namibian shelf extending to Walvis Ridge (Compton & Bergh, 2016). The Namib Desert is an important source of desert dust to the adjacent stations on the Benguela shelf compared to northern stations. The stations on the Benguela shelf are shallower and were sampled closer to the coast compared to the stations North of Walvis Ridge. The transect along the African shelf is hence sub-divided and described between

the northern non-upwelling (NORTH; ST 6–20) and shallower Benguela upwelling regions (BENG; ST 43–51 and 1–5), separated by Walvis Ridge and ABF (Figure 1).

### 2.2. Sample Collection

Sampling was carried out following GEOTRACES protocols (Cutter et al., 2010) using a dedicated GEOTRACES trace metal clean CTD rosette (Seabird), equipped with 24 Go-Flo bottles (12 L; Ocean Test Equipment) to collect full water-column depth profiles. After each cast, the Go-Flo bottles were transferred to a containerized clean-room for subsampling seawater for dTM, pTM, and other parameters. A few failed bottle closures from CTD casts resulted in no samples being collected from the respective bottles, particularly in surface waters between stations 6–8, North of Walvis Ridge. Marine particle samples were collected by filtering typically 4 L (range 0.38–6.8 L) of seawater through 0.2 µm pore-size acid cleaned polyethersulfone (PES) membrane filters (25 mm diameter, Sartorius). After filtration, samples were lightly misted with ultra-pure water (Milli-Q, Millipore) to remove salts, then transferred to acid-cleaned Petri-dishes, sealed with Parafilm, and stored frozen at −20°C until analysis in land-based facilities. The dTM samples were filtered through cartridge filters (0.2/0.8 µm Acropak-500, Pall) into acid-cleaned low-density polyethylene (LDPE) bottles, acidified to pH <2 using hydrochloric acid (UpA grade, Romil), and stored for later analysis.

In addition, surface seawater samples (~3–4 m) were collected for dTM analysis using a trace-metal clean tow-fish and a Teflon-diaphragm pump with acid-washed braided PVC tube while the ship was steaming; the waters were directly transferred into the containerized clean-room (Achterberg et al., 2001). Seawater was in-line filtered through a 0.8/0.2 µm cartridge filter (AcroPak1000, Pall) and collected into acid-cleaned 125 ml LDPE bottles, and subsequently processed identically as the samples from the trace metal clean CTD. No particulate trace metal samples were collected from the tow-fish.

### 2.3. Analytical Methods

Particulate samples were processed sequentially by leaching the filters following the protocol of Berger et al. (2008), followed by a strong acid digestion of the residual refractory material to determine L-pTM and R-pTM fractions using a method adapted from Cullen and Sherrell (1999). Briefly, the samples were processed in perfluoroalkoxy (PFA) digestion vessels (Savillex), and first leached in 2.5–3 ml of leaching reagent consisting of a weak acid (25% acetic acid, Optima grade, Fisher Scientific) and a mild reducing agent (0.02 M hydroxylamine hydrochloride, Sigma TM grade) for a total leach time of 2 hr, including a short heating step (90°C–95°C) of 10 min. Subsequently, the leachate was centrifuged, sub-sampled, and processed separately from the residual (refractory) particles. The residual leachate remaining following sub-sampling from the centrifuged samples (0.1–0.2 ml) was transferred and processed with the refractory particles, with any contributions of TMs in the transferred leachate removed from the refractory particle fraction.

The filters with residual particles were adhered to the inner wall of the digestion vessel and reflux-digested at 150°C for 15 hr in 2.5 ml of a strong acid digestion solution (50% $HNO_3$/10% HF v/v %; Optima grade, Fisher Scientific). The digestion solution was prepared with a 10 ng rhenium (Re) standard spike (Inorganic Ventures) to monitor sample loss.

Following each leach-digestion step, the respective fractions were heated to near dryness, and 0.5–1 ml of 50% $HNO_3$/15% $H_2O_2$ (v/v%) solution was added before being heated to near dryness a second time. The final residual drops (<50 µL) were re-diluted using 4.5 ml of 1 M nitric acid solution with an internal indium standard spike (1 µg/L), used as an analytical drift monitor, and stored in acid-cleaned 15 ml polypropylene tubes (MetalFree™, Labcon). The digested samples were analyzed using a high resolution inductively coupled mass spectrometer (HR-ICP-MS; Element XR, ThermoFisher) and quantified using external multi-element calibration with standards (Inorganic Ventures) prepared in a sample-matched matrix (Cullen et al., 2001).

The total particulate concentrations (T-pTM) reported are the sum of sample L-pTM and R-pTM concentrations. Blank PES filters were dipped in ultra-pure water and treated identically to sample filters, with at least two processed in each digestion batch as procedural blanks (total $n = 30$). The mean procedural blank values for each respective digestion batch was used to correct and determine sample concentrations. At least two replicates of certified reference material (BCR-414 freshwater plankton; 16.2–24.5 mg) were processed alongside the

particulate samples in each digestion batch to monitor leach consistencies and total recoveries across all digestion batches. The efficacy of the digestion procedure on the lithogenic matrix was tested by employing the refractory digestion steps, without the chemical leach, using sediment reference material (PACS-3; 17.5–34.8 mg). The procedural blank values, limits of detection, and reference material recoveries for the particulate analysis are summarized in Table S1 in Supporting Information S1.

Dissolved TM samples were measured following the procedure of Rapp et al. (2017) using HR-ICP-MS (Element XR, ThermoFisher) after offline pre-concentration of dTMs using an automated pre-concentration system (SeaFAST—Elemental Scientific) and quantified using isotope dilution (Fe, Cu, Zn, and Ni) or standard addition (Mn, Co and Pb). Dissolved TM measurements were validated using GEOTRACES GSC reference seawater (measured values 1.60 ± 0.16 nM dFe; 1.85 ± 0.34 nM dMn; 1.29 ± 0.12 nM dCu; 1.31 ± 0.15 nM dZn; 4.27 ± 0.30 nM dNi; 0.038 ± 0.04 nM dPb; $n = 8$), which were within ranges reported by Wuttig et al. (2019) (Except dCo which was slightly higher 0.117 ± 0.007 nM dCo). Dissolved aluminum was measured following the batch lumogallium method (Hydes & Liss, 1976) and validated measuring GS reference seawater (27.8 ± 0.2 nM; $n = 4$; Consensus value 27.5 ± 0.2 nM, Menzel Barraqueta et al., 2019).

Macronutrient samples ($NO_2^-$, $NO_3^-$, $PO_4^{3-}$, and $Si(OH)_4$) were collected from each Go-Flo bottle and measured on-board using segmented flow injection analysis (QuAAtro—Seal Analytical). The hydrographic parameters, including dissolved oxygen (Seabird), fluorescence (Turner Designs), turbidity (Seapoint), and beam attenuation (BAT) (WETLabs) were measured using sensors mounted on the CTD frame (Seabird SBE 9plus—Seabird). The dissolved oxygen sensor data was calibrated using discrete samples measured using the Winkler titration method (Hansen, 2007; Winkler, 1888).

Statistical analysis to determine the bivariate Pearson's correlations and principal component analysis (PCA) was carried out using OriginPro (2021) (Version 9.80) and a Microsoft Excel statistical analysis add-in software (Analyse-it® for Microsoft Excel, Version 5.66) on log-transformed data sets, which showed normal data distributions (Figure S1 in Supporting Information S1). Water column sections, station profiles, and scatterplots were prepared using Ocean Data View (Schlitzer, 2018).

### 2.4. Particle Type Indicator Elements

We used refractory particulate Al (R-pAl) as a lithogenic proxy since adsorbed Al is presumed to be removed by the labile leach, whereas lithogenic particles remain largely intact (Berger et al., 2008; Rauschenberg & Twining, 2015). Moreover, Al is more abundant and shows relatively lower variation among reported continental crust reference types than Ti (Rudnick & Gao, 2013; Taylor & McLennan, 1995). Sample R-pAl, R-pTi, and R-pFe elemental ratios were used to distinguish among lithogenic sources by comparing them to available regional lithogenic references (Table S2 in Supporting Information S1).

The labile particulate pool includes amorphous and readily reducible Mn bio-oxyhydroxides (hereafter *Mn oxides*) and Fe oxy-hydroxides (hereafter *Fe oxides*), adsorbed TMs, and intracellular biogenic pTMs, which are dissolved by the chemical leach (Berger et al., 2008; Rauschenberg & Twining, 2015; Twining et al., 2015). These particulate phases are referred to within the L-pTM fraction.

Phosphorus is primarily associated with organic (biogenic) particles, and hence total particulate phosphorus (pP) was selected as an indicator of biogenic particles. Biominerals, such as biogenic silica and calcium carbonate, and particulate organic carbon (POC) were not analyzed.

## 3. Results and Discussions

### 3.1. Hydrographic Features

The main water masses along the transect were defined using isopycnal densities calculated using salinity and potential temperature measurements (Rahlf, 2020). The section of the water column north of Walvis Ridge comprised of Tropical Surface Water (TSW) in the top 20 m and Subtropical Underwater (STUW) in the subsurface mixed layer (20–50 m), which was underlain by South Atlantic Central Water (SACW) between 50 and 500 m. The deeper water masses in the Angola Basin included Antarctic Intermediate Water (AAIW) between ~500 and 1,200 m, Upper Circumpolar Deep Water (UCDW) between ~1,200 and 2,000 m, and North Atlantic

Deep Water (NADW) between 2000 and 4,500 m (Figure 2a). Upwelling of colder (15°C–18°C) and less saline (~35) SACW was observed between 15.8°S and 28.7°S at the southern Benguela shelf stations (ST 45–51 and 1–5), including the Lüderitz cell (ST 49–51; 23°S–25.5°S) (Rahlf, 2020; Rahlf et al., 2020, 2021), which is the most intense wind-driven upwelling cell in the world's ocean (Lutjeharms & Meeuwis, 1987). Enhanced primary production supported by upwelled nutrient-rich waters was evident by increased fluorescence (Figure 2d). The Congo River plume signal was confined primarily within the TSW layer (<20 m), which persisted as far south as station 8 and northwest as far as station 22 (up to 1,000 km from the Congo River mouth), evident in the salinity, radium and dAl distributions (Menzel Barraqueta et al., 2019; Vieira et al., 2020).

An OMZ (<50 μM oxygen) persisted along the transect extending from the Benguela shelf into the northern open ocean transect (Figure 2b). Oxygen concentrations decreased with depth (~25–200 m) on the Benguela shelf (BENG) extending to (near-)bottom waters (≤50 m from bottom), and the lowest oxygen concentrations (<4 μM) were recorded within the Lüderitz cell (ST 49–51; 23–25.5°S). The sediments underlying the BENG upwelling stations are reported to be anoxic, with several stations near locations where sulfidic sediments were also reported (e.g., ST 49–51 < 50 km away) (Böning et al., 2020; Borchers et al., 2005; Govin et al., 2012). A less intense oxygen minimum layer (<100 μM oxygen) persisted at the NORTH latitudinal coastal transect stations (ST 6–16) primarily within SACW between ~50 and 600 m with concentrations down to 20 μM. The oxygen minimum layer extended off the shelf and into the open ocean (3°S; ST 17–24) between ~200 and 500 m, with dissolved oxygen as low as 40.5 μM.

### 3.2. Particulate Trace Metal Distribution Patterns

The T-pTM concentrations varied over orders of magnitude between $10^{-2}$ to $10^{7}$ pM, with mean concentrations decreasing in the order Al-P > Fe > Ti-Mn > Zn > Cu-Ni > Co > Cd-Pb (Figures S3 and S4 in Supporting Information S1). Most of the maximum concentrations of pTMs occurred in the bottom waters of the shallow coastal station 45 with concentrations reaching up to 5.11 μM pAl, 1.70 μM pFe, 138 nM pTi, 10.0 nM pMn, 3.19 nM pZn, 1.58 nM pNi, 438 pM pCo, 204 pM pPb, and 129 pM pCd (Figure S4 in Supporting Information S1). The highest concentration of pP was 253 nM at station 6 (11 m), and pCu was 1.33 nM at station 3 (69 m) (Figure S4 in Supporting Information S1). The T-pTM (pP, pCo, pFe, and pMn) concentrations at stations 6 and 7 were similar to values from a nearby station reported by Noble et al. (2012) collected in 2007 during the same season (Gac01-ST 19—Figure S5 in Supporting Information S1). The pTM ranges were also comparable to other shelf and slope regions in the Pacific, Arctic, North and South Atlantic Oceans (Table S3 in Supporting Information S1). Sections of L-pTMs and R-pTMs are shown in Figures 3 and 4, respectively.

The mean labile fractions of T-pTMs were greater than 80% for Mn, Cd, Zn, and Pb, between 53% and 59% for Co, Ni, and Cu, around 41% for P, 25% for Fe, 19% for Al, and 1% for Ti (Figure 5). These observations are consistent with ranges reported elsewhere using the same chemical leach (e.g., Milne et al., 2017; Rauschenberg & Twining, 2015; Twining et al., 2019) (Table S4 in Supporting Information S1). An exception was pP, which was comparatively less labile in the current study compared with previous work, and R-pP was attributed primarily to residual (refractory) biogenic particles (see Section 3.3). The labile pTM fractions generally decreased where the lithogenic particle abundance (R-pAl concentrations) increased, and refractory pTMs (primarily lithogenic particles) dominated the pTM pool (van der Merwe et al., 2019), particularly for pAl, pPb, pCo, pCu, and pNi across the transect, and for pMn only below the photic zone on the Benguela shelf (Figure 5).

In the deeper NORTH stations (ST 6–11) and along the open ocean transect (ST 21–24), enhanced L-pAl/T-pAl fractions (up to 79.8%) were apparent only in (sub-)surface waters (≤350 m), with no enhanced L-pAl/T-pAl fractions below 2,000 m (Figure 5). The vertical concentration profiles of pCu, however, exhibited increasing labile fractions (52%–78% L-pCu) and concentrations (13–47 pM L-pCu) at depths >2,000 m (Figures 3 and 5), where lithogenic particle concentrations were also relatively low (9.87 ± 12.8 nM R-pAl; $n = 23$). The enhanced L-pCu fractions coincided with increases in dCu concentrations (up to 2.95 nM), indicating scavenging onto particulate phases (Bruland, 1980; Little et al., 2013, 2018), specifically within NADW (>27.8 kg $m^{-3}$ $\sigma_\Theta$).

A PCA was conducted on log-transformed data for each particulate fraction for which full elemental and ancillary data were available (Figure S6 in Supporting Information S1). PC1 explained 50.1%, 36.8%, and 40.4% of the total variance of T-pTM, L-pTM, and R-pTM, respectively, and is associated with lithogenic particles, capturing 71%–86% of the individual variance of R-pAl. PC2 explained 16.7%, 22%, 18.2% of total variance of T-pTM,

10.1029/2022GB007453

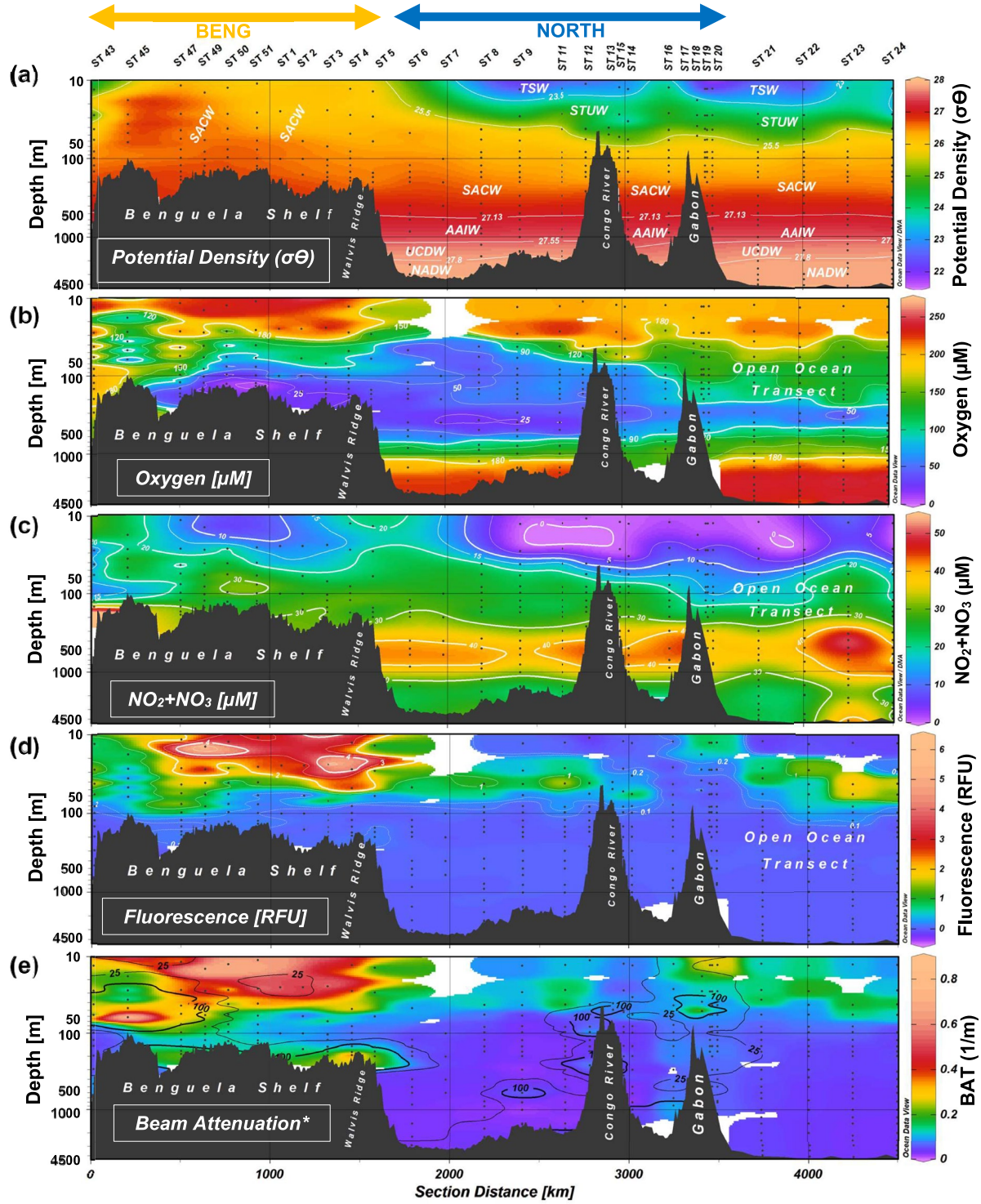


**Figure 2.** Main hydrographic features along the GA08 transect. Sections of (a) potential density of seawater with main water masses in the study region; TSW = Tropical Surface Water; STUW = Subtropical Underwater; SACW = South Atlantic Central Water; AAIW = Antarctic Intermediate Waters; UCDW = Upper Circumpolar Deep Water; NADW = North Atlantic Deep Water. (b) Dissolved oxygen concentrations. (c) Nitrate + nitrite concentrations. (d) Fluorescence in Relative Fluorescence Units (RFU). (e) Beam Attenuation (BAT) in fractional attenuance per meter. Contour lines represent measurement intervals of each respective analyte, except (e), which are of refractory particulate Al (R-pAl) concentrations (nM). Note the logarithmic depth scales. Vertical labels used for stations 11–20 are to help distinguish between the stations that were close together and do not signify a categorical difference between stations.

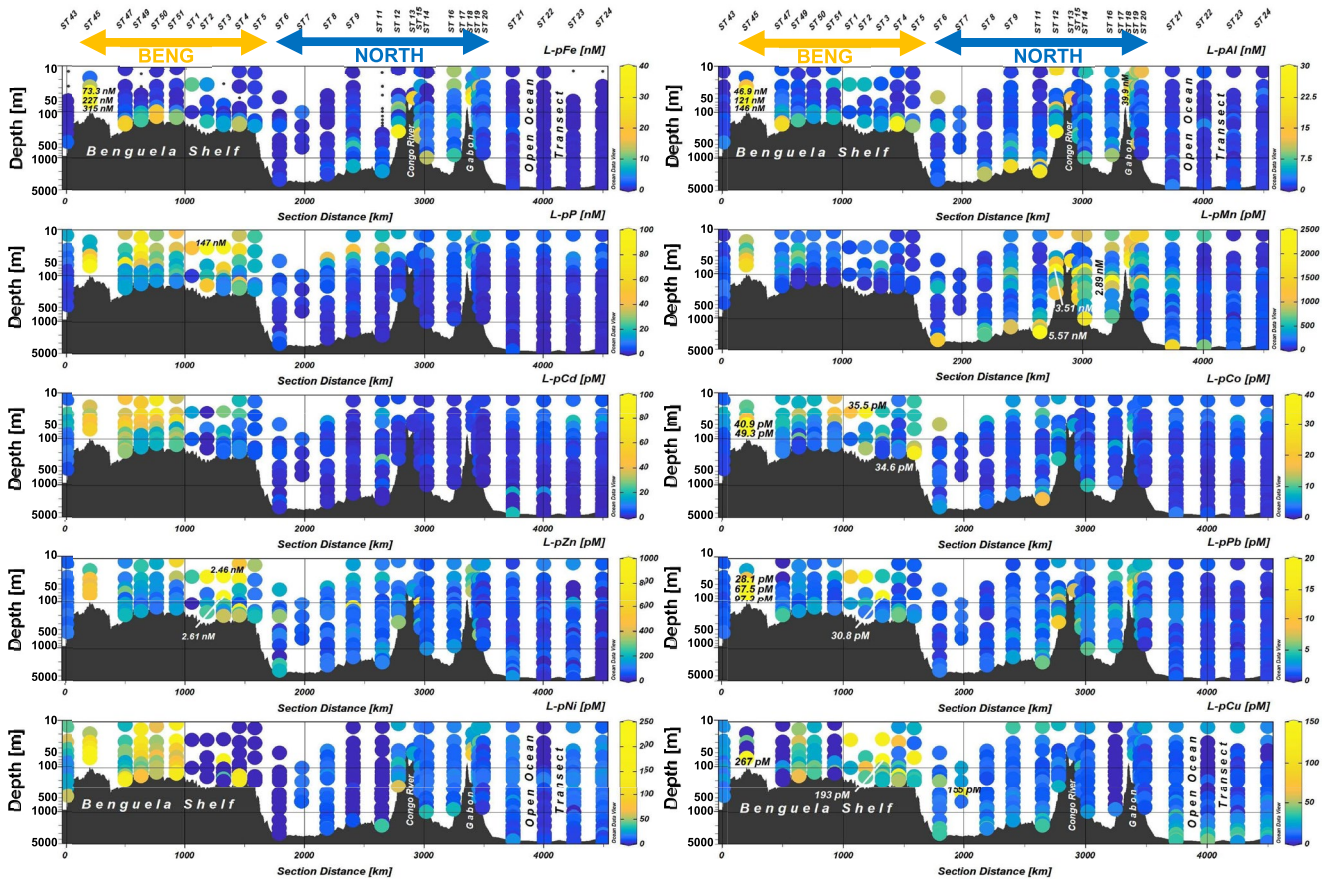


**Figure 3.** Distribution of labile particulate trace metals (L-pTMs) across the GA08 transect. Note the logarithmic depth scales. One anomalously high measurement was excluded a priori (>7.1 nM L-pCu; ST 2; 25 m). Concentrations have been annotated where values exceeded the color-bar scale (*z*-axis).

L-pTM and R-pTM, respectively, and is associated with biogenic particles, capturing 70%–77% and 63%–74% individual variance of fluorescence and T-pP, respectively. Despite their association to biogenic particles, only minor variances of several bio-essential L-pTMs (Zn, Cu, Ni, Cd, and Co; which are largely solubilized by the leach) were captured by PC2, with almost none for L-pCu and L-pZn (see Section 3.3 below). This may be due to the variances of these L-pTMs being more closely associated with other abiogenic, non-lithogenic particulate phases, such as a scavenged phase, and by spatial (regional) contrasts in their concentrations (see Section 3.2.1). PC4, PC5, and PC6 only captured relatively large variances for individual elements, specifically L-pZn, L-pCu, and L-pCd (81.4%, 69.4%, and 26.5% combined individual variances, respectively), likely reflecting variances arising from regional differences, with significant individual variance also captured for R-pTMs Ni (PC4: 60.7%), Cu (PC5: 54.5%), and Mn (PC6: 31.8%). PC variances that were largely exclusive to pCu are also reported for pTM data sets from the North Atlantic (Ohnemus & Lam, 2015). PC3 (8.6%–10.2% total variance) captured the greatest individual variance for oxygen (48%–71%), with only significant associations with L-pCo (35%), R-pCd (30%), T-pMn (15%), and R-pZn (15%). No variance of the Mn oxide proxy, L-pMn, was captured within the third principal component of the L-pTM data set analysis. However, relatively high variances for dFe (29%–35%) were captured by PC3 in all pTM data sets.

The distributions of labile and refractory pTMs showed distinct regional and biogeochemical variations along the transect, including: (a) A contrasting biogenic particle abundance between BENG (upwelling) and NORTH (non-upwelling) stations; (b) Contrasting refractory (lithogenic) particle compositions on the Benguela Shelf and stations north of Walvis Ridge; (c) Distinct Fe and Mn cycling within the oxygen-depleted waters on the Benguela Shelf (d) Increased adsorption of TMs onto particles in the Congo River plume. The regional and biogeochemical variations will be discussed in the following sections.

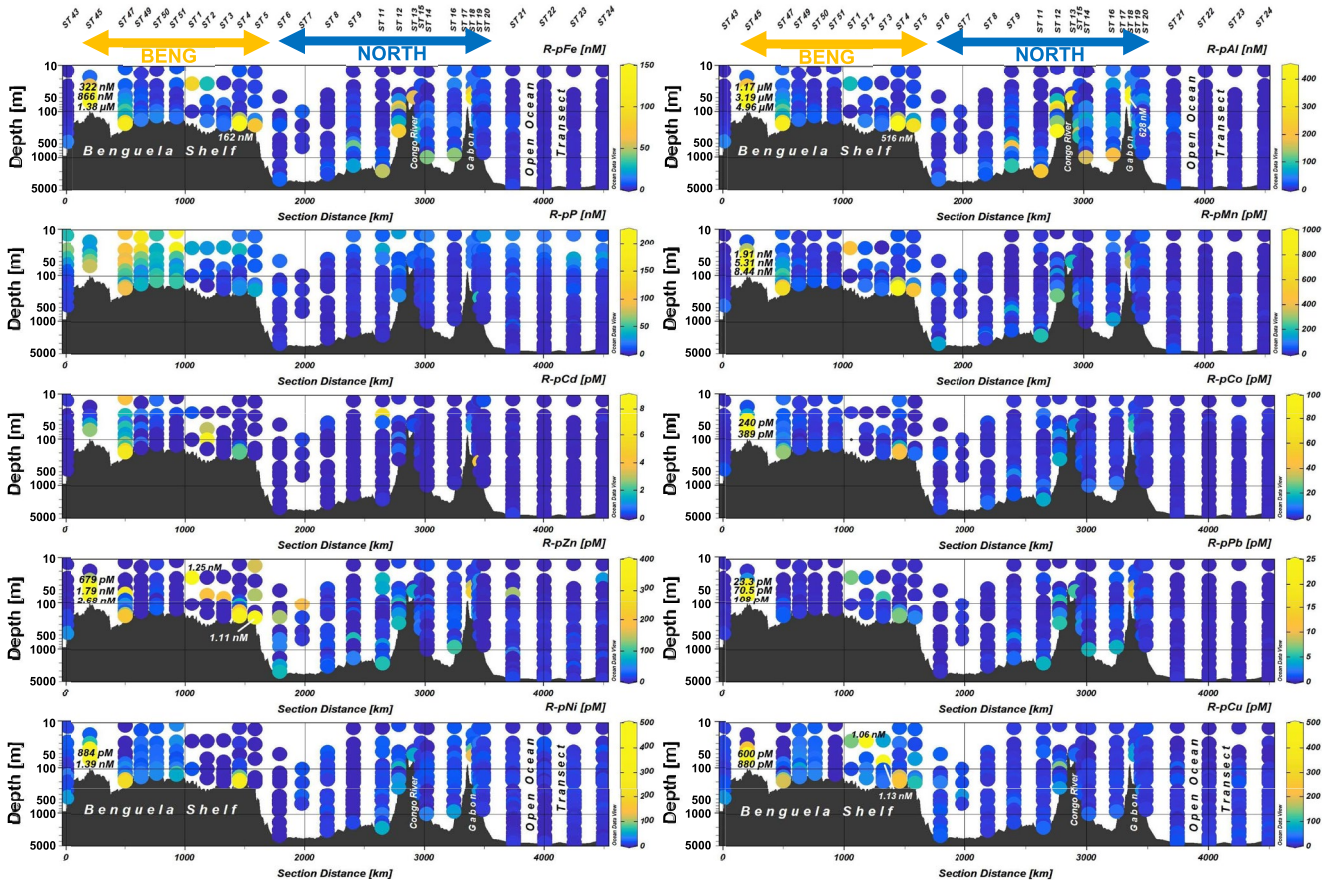


**Figure 4.** Distribution of refractory particulate trace metals (R-pTMs) across the GA08 transect. Note the logarithmic depth scales. One anomalously high measurement was excluded a priori (>1 nM R-pPb; ST 6; 196 m). Concentrations have been annotated where values exceeded the color-bar scale (*z*-axis).

### 3.2.1. Bio-Essential Particulate Trace Metals

Concentrations of bio-essential TMs (Zn, Cu, Ni, Cd, Co, and also P) in the L-pTM and R-pTM fractions were higher in the BENG region compared to the NORTH (*t*-test; $p < 0.01$ and <0.05, respectively; except R-pCo) (Table S5 in Supporting Information S1). This was attributed to the enhanced primary production (i.e., increased (bio-) assimilation of essential TMs) within BUS where concentrations of the biogenic particle indicator pP were up to 5-fold higher in the BENG region (ST 43–51 and 1–5) compared to NORTH (ST 6–20), reaching 253 nM T-pP (147 nM L-pP). Maximum bio-essential L-pTM concentrations in the BENG and (NORTH, in brackets) regions were 2.61 nM (0.81 nM) L-pZn, 228 pM (87.4 pM) L-pNi, 193 pM (155 pM) L-pCu, 74.3 pM (26.4 pM) L-pCd, and 35.3 pM (16.7 pM) L-pCo (Figure 3), excluding station 45. The vertical distributions of bio-essential L-pTMs (Zn, Cu, Ni, Cd, Co, and also P) and R-pP showed highest concentrations in surface waters and decreased with depth along the transect (Figure 3), coinciding with enhanced fluorescence (Figure 2d), implying phytoplankton sources.

Bio-essential R-pTMs (and also Pb; discussed in Section 3.3) were co-distributed with R-pAl with good correlations ($r = 0.56$–$0.97$; $p < 0.01$; Table S6 in Supporting Information S1), implying a lithogenic source. Moreover, bio-essential R-pTMs in the top 100 m showed higher correlations with R-pAl ($r = 0.925$–$0.996$) than with R-pP ($r = 0.172$–$0.395$) (Figure S7 in Supporting Information S1). The exceptions were R-pP and R-pCd, which showed lower correlations with R-pAl ($r = 0.18$ and 0.42, respectively; Table S6 in Supporting Information S1) but correlated well with each other ($r = 0.73$; $p < 0.001$; Table S6 in Supporting Information S1) and were associated with refractory (residual) biogenic particles (see Section 3.3).

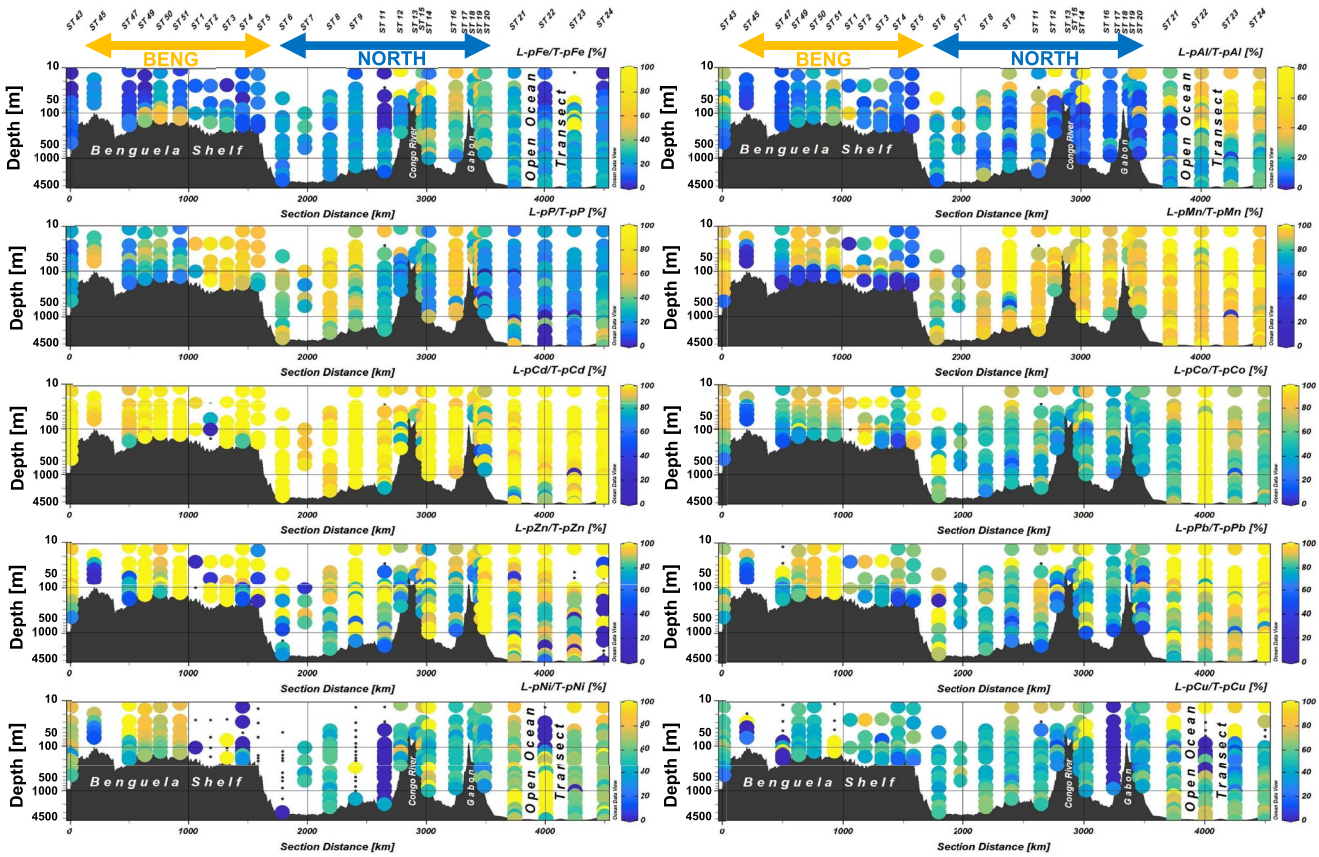


**Figure 5.** Distribution of labile particulate fraction (%) of total particulate trace metals across the GA08 transect. Contour lines indicate where refractory particulate Al (R-pAl) is ≥25 nM (thin) or ≥100 nM (thick). Note the logarithmic depth and different color scales for each element.

### 3.2.2. Lithogenic Particulate Trace Metals

Concentrations of particulate lithogenic elements (Al, Ti, and Fe) showed no statistical difference among regions (Table S5 in Supporting Information S1). Lithogenic pTMs concentrations were generally lower in surface waters (<20 nM R-pAl; ≤50 m), except in the Congo plume (ST 16–20; 12.2–443 nM R-pAl), at some BENG stations (ST 47, 1, and 2; 30.9–85.3 nM R-pAl), and at shallow stations 13 (59 m) and 45 (68 m) (295 nM and 3.19 μM R-pAl, respectively) (Figure 4). Concentrations of lithogenic particles (i.e., R-pAl) were primarily enhanced in (near-)bottom waters, consistent with benthic resuspension and nepheloid layer distribution patterns. Elevated lithogenic particle concentrations were observed within 100 m from the seafloor at stations 9 and 11 (up to 97 and 227 nM R-pAl, respectively), and at shallower shelf stations 12 (289 m) and 17 (53 m) (up to 469 and 628 nM R-pAl, respectively). The highest lithogenic pTM concentrations were at the shallow coastal station 45, with 4.96 μM R-pAl (145 nM L-pAl), 1.38 μM R-pFe (314 nM L-pFe), and 138 nM R-pTi (138 pM L-pTi), and the lowest concentrations were in deep waters between Walvis Ridge and the Congo River shelf (ST 6–11), and in the open ocean (ST 22–24; <5 nM R-pAl) (Figures 3 and 4). Labile particulate Pb, Al, Ti, Mn, and Fe concentrations were also enhanced where R-pAl concentrations were high, as reflected by their close correlations with R-pAl ($r = 0.61–0.91$; $p < 0.001$) (Table S6 in Supporting Information S1), implying common (benthic) sources.

## 3.3. Biogenic Particles

BAT and turbidity, used as a proxy for particulate matter, were enhanced primarily in surface waters and highest in the Benguela upwelling region (Figure 2e and Figure S8 in Supporting Information S1), and strongly correlated with the biogenic particle indicator, T-pP ($r = 0.868$ and 0.774, respectively; Figures S9a and S9c in Supporting Information S1) and with fluorescence in the surface waters ($r = 0.770$, <100 m). T-pP in surface samples showed slightly higher correlations with BAT ($r = 0.868$; <100 m; Figure S9a in Supporting Information S1),

compared to turbidity ($r = 0.774$; <100 m), and enhanced BAT measurements were more pronounced in surface samples compared to turbidity (Figure S9e in Supporting Information S1). This observation is consistent with other studies that reported enhanced BAT largely resulting from enhanced particulate organic matter concentrations (e.g., Bishop et al., 2004; Lam & Bishop, 2008; Noble et al., 2012; Ohnemus et al., 2018).

Particulate P concentrations, in all fractions, were highest in the euphotic zone (<50 m) and sharply decreased with depth along the transect, generally following the same vertical profiles as fluorescence (Figures S2 and S4 in Supporting Information S1). Higher L-pP and R-pP concentrations persisted deeper into the BENG water column compared to the NORTH (Figures 3 and 4), reflecting longer remineralization length scales due to increased biogenic particle production, oxygen deficiency with lower remineralization rates (Weber & Bianchi, 2020), increased particle ballasting with enhanced sinking rates (Armstrong et al., 2001; Klaas & Archer, 2002), or a combination thereof. Significant contributors of ballast to particle aggregates within the BENG upwelling stations likely include dust from the nearby Namib Desert and settling biominerals associated with the increase in primary production.

The mean L-pP/T-pP fractions in (sub-)surface waters (<200 m) were 39.7% ± 20.7% ($n = 206$) along the entire transect, which were notably lower than labile fractions from other regions reporting average L-pP/T-pP fractions of ∼70–80% (e.g., Rauschenberg & Twining, 2015; Twining et al., 2015). L-pP/T-pP fractions varied (spatially) between stations, with some stations exhibiting higher L-pP/T-pP fractions (up to 84.8%) that were more consistent with labile fractions reported from other areas, such as between stations 1–9 (67 ± 14%; ≤100 m; $n = 25$).

Increasing biogenic or lithogenic particle loads did not affect the percentage leached from biogenic particles, as indicated by the weak correlations of L-pP fractions (%) with T-pP and R-pAl concentrations over several orders of magnitude ($r = 0.04$ and 0.06, respectively; top 300 m) (Figure S10 in Supporting Information S1). While it may be argued that the lower L-pP/T-pP fractions may reflect the inclusion of refractory inorganic pP phases, areas where inorganic pP would possibly be higher such as in (near-)bottom samples of the Benguela shelf where phosphorite deposits are documented (Compton & Bergh, 2016), did not show a significant contribution to the pP pool. This was indicated by the low co-occurring levels of lithogenic elements (R-pAl and R-pTi), which were also low where R-pP was highest (i.e., in surface waters; Figure 4). Furthermore, phosphorites included in particulate samples are potentially chemically labile (Jian-rui & Jie, 2016; Porto et al., 2018). Therefore, the R-pP pool through the transect was ascribed primarily to residual (more refractory) biogenic particle phases. Notable exceptions were at station 45 (1.17–4.96 μM R-pAl), and in the bottom waters of stations 4 and 5 (58.5–516 nM R-pAl), where lithogenic element concentrations were particularly high.

Bio-essential pTMs (Cd, Ni, Co, Cu, and Zn) correlated well with pP in both labile ($r = 0.63$–$0.79$) and total particulate ($r = 0.52$–$0.79$; except T-pZn) fractions in the top 100 m (Figure S11 in Supporting Information S1). Additionally, sample T-pTM:T-pP ratios (upper and lower quartile value ranges) and linear regression slopes of surface samples (<100 m) were consistent with ranges of reported plankton stoichiometries (Table 1 and Figure S11 in Supporting Information S1). This supports the assumption that T-pP was primarily associated with biogenic sources, and therefore a suitable biogenic particle indicator along this transect, also implying that these bio-essential pTMs were primarily associated with biogenic materials. Interestingly, however, the sample L-pTM:L-pP ratios (upper and lower quartile values, and linear regression slope values) of the bio-essential elements were comparatively higher than their respective T-pTM:T-pP ratios, which were at the upper limit of or slightly exceeded reported plankton values from other regions (Table 1). This suggested that the pTMs associated with biogenic particles were either comparatively more labile than biogenic pP, or that biogenic pP was (variably) more resistant to the applied leach, with the latter case providing an explanation for the persistence of R-pP in surface waters and biogenic particle-like vertical profiles through the water column.

The spatial fluctuations in L-pP/T-pP fractions are suspected to have varied as dominant taxa in bulk phytoplankton communities shifted between stations, reflecting differential lability of pP among different (dominant) phytoplankton groups. This was inferred using phytoplankton taxa assemblage data from this cruise which were reported by Browning et al. (2017) ($n = 5$ stations along the transect of this study). In regions influenced by upwelling, diatoms dominated the bulk plankton assemblages (fraction of total chlorophyll-a) and generally coincided with elevated L-pP fractions, particularly in surface waters between stations 2–5 (58%–84% L-pP fraction of total pP). Increased L-pP fractions continued to persist where diatoms comprised an important fraction of the bulk plankton assemblages (about one-third) in between stations 8–9 (up to 84.5% L-pP/T-pP) and stations 16–20 (up to 69% L-pP/T-pP). In contrast, where haptophytes dominated the plankton assemblage, away from

**Table 1**
*Compiled Plankton Reference Trace Metal Stoichiometries Compared to Samples From the Top 100 m of the GA08 Transect*

| Reference Source | TM:P ratio (mmol:mol) | | | | | | |
|---|---|---|---|---|---|---|---|
| | Fe | Mn | Zn | Ni | Cu | Cd | Co |
| **North Atlantic Ocean (Trichodesmium)** (Nuester et al., 2012; Tovar-Sanchez et al., 2006) | 5–31 | 1–5 | 0.2–13 | 1–8 | 0.4–2.1 | 0.02–0.31 | 0.01–0.15 |
| **Equatorial Pacific Ocean (Phytoplankton)** (Twining et al., 2011) | 1.9–8.4 | 0.49–0.58 | – | 1.0–1.2 | – | – | 0.06–0.07 |
| **Culture (Average Eukaryotic Phytoplankton-15 species)** (Ho et al., 2003) | 7.5 | 3.8 | 0.8 | – | 0.38 | 0.21 | 0.19 |
| **Southern Ocean (Large Diatoms)** (Cullen et al., 2003) | – | 1.7 | 11.1 | – | 1.44 | 1.29 | 0.15 |
| **North Atlantic Ocean (mostly Flagellated cells)** (Kuss & Kremling, 1999) | 4.6 | 1.6 | 1.9 | 1.4 | 0.37 | 0.51 | 0.19 |
| **Equatorial Pacific Ocean (mostly Zooplankton)** (Collier & Edmond, 1984) | 4.9 | 0.35 | 3.2 | 0.97 | 0.48 | 0.56 | – |
| **Southern Ocean (Large Diatoms)** (Collier & Edmond, 1984) | – | – | 13.3 | 0.68 | 2 | 0.07 | – |
| **Northeast Atlantic Spring Bloom (picoplankton and coccolithophores)** (Klein et al., 2013) | 9.1–9.8 | – | – | – | 0.27–0.52 | 0.06–0.07 | 0.04–0.06 |
| **Eastern Tropical South Pacific (near Peruvian Coast)** (Ohnemus et al., 2017) | 39.7 | 1.0 | 1.0 ± 0.88 | 0.54 ± 0.39 | 0.40 ± 0.37 | 0.54 ± 0.24 | 0.08 ± 0.05 |
| **GA08 (All ≤100 m) ($n$ = 131) (this study)** | | | | | | | |
| **T-pTM:T-pP** | **(–)** | **(–)** | **(–)** | **(0.46)** | **(0.50)** | **(0.27)** | **(0.10)** |
| L-pTM:L-pP | (–) | (–) | (8.7) | (1.6) | (0.96) | (0.57) | (0.21) |
| **GA08 (BENG—ST 43–51 and 1–5 ≤ 100 m) ($n$ = 46) (this study)** | | | | | | | |
| **T-pTM:T-pP** | **36.5–214** | **1.8–8.1** | **1.6–8.7** | **0.66–1.7** | **0.69–2.11** | **0.24–0.51** | **0.09–0.23** |
| L-pTM:L-pP | 14.5–146 | 4.5–14.6 | 4.9–11 | 1.9–3.8 | 0.86–2.6 | 0.59–2.1 | 0.13–0.47 |
| **GA08 (NORTH—ST 6–24 ≤ 100 m) ($n$ = 85) (this study)** | | | | | | | |
| **T-pTM:T-pP** | **42.2–953** | **7.1–49.6** | **4.3–9.2** | **0.96–2.8** | **0.97–2.1** | **0.10–0.31** | **0.15–0.32** |
| L-pTM:L-pP | 33.0–916 | 21.6–134 | 9.1–27.7 | 2.2–4.5 | 1.3–3.7 | 0.26–0.96 | 0.25–0.62 |

*Note*. Concentration ranges referenced from this study are the upper and lower quartile values of individual sample labile particulate trace metal (L-pTM): labile particulate phosphorus (L-pP) ratios (mmol:mol) and total particulate TM (T-pTM): T-pP ratios. GA08 values reported in brackets are linear regression slope values, shown for elements where $r$ is ≥0.5, and bold values represent the T-pTM:T-pP fractions, while unformatted values represent L-pTM:L-pP fractions. Table adapted from Twining and Baines (2013).

upwelling regions, lower L-pP fractions were generally observed, such as in the southernmost coastal region on the Benguela shelf (11.9%–56.5% L-pP of total pP; ST 45–50 < 100 m). The lowest L-pP fractions that were generally observed in surface waters between stations 21–24 (14.8%–28.4% L-pP of total pP; <100 m), where haptophytes and *Prochlorococcus* equally comprised about one-third, each, of the community assemblage, with almost no diatoms present.

Differential remineralization length scales of bio-essential elements through the water column, attributed to variable lability of respectively associated (intra-)cellular components, have been described using synchrotron X-ray fluorescence mapping by Twining et al. (2014), focused on diatoms. Given the similarity of bio-essential T-pTM:T-pP ratios to plankton reference sources in surface waters along the transect (Table 1), but variable L-pP/T-pP fractions (Figure 5), we postulate that it is plausible that the lability of biogenic pP is also variable between different phytoplankton taxa. This assumption is based on indirect evidence, further exploration of pP (and pTM) lability of different phytoplankton taxa is warranted in future studies to confirm and expand on this hypothesis.

Nonetheless, refractory particulate phases represent the particulate fraction that will persist in the water column on longer timescales, compared to the L-pTM fractions, as they settle or are laterally transported away from

their sources. This also implicates pP cycling, particularly over the Benguela shelf, as it would directly imply that (biogenic) R-pP from settling particles are a potentially significant source of refractory pP to the underlying seafloor, contributing to the enriched pP documented on the Benguela shelf (Compton & Bergh, 2016).

Samples from the NORTH stations (ST 6–20) exhibited higher labile and total bio-essential pTMs:pP ratios in the top 100 m compared to the BENG stations, except for pCd, which was higher in the BENG region (Table 1 and Figure S13 in Supporting Information S1). This is possibly due to the partial inclusion of other abiotic L-pTM phases (i.e., adsorbed, and precipitated phases) into the L-pTM pool and/or higher intracellular TM:P quotas associated with the above described, differing bulk plankton community structures along the transect. Some TMs released in solution following the remineralization of biogenic particles are susceptible to (re-)adsorption onto particle surfaces, such as Cu (Boyle et al., 1977; Bruland, 1980; Bruland et al., 2014; Little et al., 2013, 2018; Richon & Tagliabue, 2019), and Ni, Co, and Zn (Archer et al., 2020; Weber et al., 2018; Zheng et al., 2021). Therefore, increased adsorption of these TMs onto particles is more likely to occur where dTM concentrations were high, as in the river-influenced stations in the NORTH region (see Section 3.6), and where higher concentrations of labile authigenic phases were present (i.e., Fe and Mn oxides), where enhanced biogenic L-pTM:L-pP ratios were observed (Figure S13 in Supporting Information S1).

The pCo:pP ratios in waters <50 m were very similar in the BENG (0.09–0.24 and 0.14–0.55 mmol:mol T-pCo:T-pP and L-pCo:L-pP, respectively; lower and upper quartile values; $n = 25$) and NORTH (0.13–0.24 and 0.20–0.53 mmol:mol T-pCo:T-pP and L-pCo:L-pP, respectively; lower and upper quartile values; $n = 40$) regions (Figures S13b and S13g in Supporting Information S1), where biogenic particle abundance was highest. Also, the pCo:pP ratios were within the same order of magnitude of reported plankton ranges (Table 1). This suggests that the pCo pool was most likely associated with biogenic particles, and that abiotic phases (i.e., Co adsorbed onto particles) were not a major fraction of the L-pCo pool in surface waters (≤50 m). However, waters at depths between 50 and 100 m exhibited higher pCo:pP ratios (0.19–0.38 and 0.29–0.79 mmol:mol T-pCo:T-pP and L-pCo:L-pP, respectively; lower and upper quartile values; $n = 41$), and showed close correlations between L-pCo and L-pMn ($r = 0.827$; ST 6–24; $n = 41$), implying that L-pCo and L-pMn were largely associated with the same labile particulate phases (i.e., Mn oxides), which is consistent with co-precipitation of Co and Mn, during Mn (bio-)oxidation (Cowen & Bruland, 1985; Moffett & Ho, 1996; Tebo et al., 2004, 2005).

Particulate Fe and Mn, in labile and total particulate fractions, showed weak correlations with pP ($r < 0.1$; ≤100 m; Figure S12 in Supporting Information S1), with much higher individual sample labile and total pTM:pP ratios compared to reported plankton stoichiometry ranges (Table 1). This is likely due to an increased fraction of co-occurring labile abiogenic pTM phases (such as adsorbed Fe and Mn, and labile Fe and Mn oxides) as part of the labile particulate fraction, masking the biogenic L-pTM pool, which were enhanced with lithogenic (benthic) sources, as implied through their closer correlations with R-pAl ($r = 0.64$–$0.82$; Figure S12 in Supporting Information S1) (see Sections 3.4–3.6).

The enhanced labile fractions of pAl observed in the top 350 m of the water column at the NORTH and open ocean stations (up to 74%; ST 6–24; Figure 5) were associated with increased adsorption of Al, possibly onto biogenic silica (i.e., opal) or other particles, and/or the inclusion of other labile L-pAl phases, such as aluminum oxyhydroxides (Berger et al., 2008). Samples that were deeper showed much lower L-pAl fractions (14.8% ± 7.4%; Max 33.1%; ≥350 m; $n = 92$), as biogenic particle (opal) fractions tend to decrease with depth due to dissolution (Lam, Ohnemus, & Auro, 2015; Lam et al., 2018; Xiang & Lam, 2020). While biogenic silica was not measured in samples of this study, other studies across the Atlantic, Indian, and Southern oceans, as well as in mesocosm experiments have shown preferential Al adsorption onto biogenic silica (Barrett et al., 2018; Menzel Barraqueta et al., 2018; Middag et al., 2015; Moran & Moore, 1988; Orians & Bruland, 1986). Diatom abundances were apparently low in open ocean stations (ST 21–24), as inferred above, we can only speculate that enhanced L-pAl/T-pAl fractions in these samples (Figure 5) may reflect the inclusion of a relatively higher fraction of labile aluminum oxyhydroxides, adsorption onto other particles, or inclusion of other L-pAl phases.

At first glance, the significant L-pPb variance (57%; Figure S6 in Supporting Information S1) captured by PC2 of the L-pTM data set (associated with biogenic particles) suggests enhanced Pb adsorption onto biogenic particles. However, correlations between L-pPb and R-pAl (lithogenic proxy) ($r = 0.95$; $n = 132$) were stronger in the top 100 m, where biogenic particle abundances were highest, compared to L-pP ($r = 0.44$; $n = 132$) (Figure S14 in Supporting Information S1). L-pPb also exhibited better correlations with L-pFe and L-pMn ($r = 0.81$ and $r = 0.66$, respectively, Table S6 in Supporting Information S1). The closer correlations of L-pPb with the

other particle proxies suggested that the affinity for Pb adsorption was higher onto other co-occurring (abiogenic) particles, such as lithogenic particles (Chen, Boyle, et al., 2016; Rutgers Van Der Loeff & Boudreau, 1997), and/or Fe and Mn oxides (Allen et al., 1990; Boyle et al., 2005; Fernex et al., 1992; Ohnemus & Lam, 2015; Rapp et al., 2019; Rusiecka et al., 2018; Sherrell & Boyle, 1992). However, Pb adsorption onto biogenic particles cannot be discounted and has been implicated in observations in the North Atlantic and Southern Ocean (Cochran et al., 1990; Schlosser & Garbe-Schönberg, 2019), North Pacific (Cochran et al., 1990; Nozaki et al., 1976), and in laboratory studies (Chuang et al., 2014; Yang et al., 2015).

### 3.4. Lithogenic Particles

Turbidity and BAT were enhanced in (near-)bottom waters (Figure 2e and Figure S8 in Supporting Information S1) where very high concentrations of the lithogenic proxy, R-pAl, were observed. Increased lithogenic particle (R-pAl) concentrations exhibited higher correlations with turbidity measurements ($r = 0.703$; >100 m; Figure S9d in Supporting Information S1) than BAT ($r = 0.677$; >100 m; Figure S9b in Supporting Information S1), and enhancements in the turbidity signals were more pronounced in samples below the surface (>100 m), compared to BAT (Figure S9e in Supporting Information S1). This suggests that lithogenic particles exhibited a higher influence on turbidity signals compared to BAT.

Refractory particles from the BENG region were distinctly enriched in R-pFe (Figure 6b and Table S2 in Supporting Information S1), showing higher R-pFe:R-pAl and R-pFe:R-pTi ratios (0.276 and 9.90 mol:mol, respectively; linear regression slope values), compared to samples from the NORTH region (0.186 and 7.66 mol:mol, respectively; linear regression slope values) ($t$-test $p < 0.05$; Table S7 in Supporting Information S1) and upper continental crust (UCC) reference sources (0.232 and 8.77 mol:mol, respectively; Rudnick & Gao, 2013). The higher R-pFe abundances in BENG region samples are partially attributed to local sources of sediment resuspension (Böning et al., 2020; Borchers et al., 2005; Govin et al., 2012) and the Namib dust (Annegarn et al., 1983; Eltayeb et al., 1993), which are enriched in Fe (Table S2 in Supporting Information S1). The presence of Fe sulfides and biotite in resuspended sediment particles, as reported for the Benguela shelf (Böning et al., 2020; Bremner & Willis, 1993), can contribute to R-pFe enrichment relative to R-pAl and R-pTi. Additionally, Fe-sulfide precipitation within microenvironments of organic-rich particle aggregates within the oxygen-deficient waters of the BENG region (Bianchi et al., 2018) may possibly contribute to the increased R-pFe (Bianchi et al., 2018). Indeed, elevated R-pFe:R-pAl ratios (0.43–0.72, mol:mol) in (near-)bottom water samples of the most oxygen-depleted waters on the Benguela shelf (<10 μM oxygen; ST 49–51) were consistent with the inclusion of benthic particles (0.90 Fe:Al was reported in sediment at a nearby location at 14.4°E, 25.0°S; Böning et al., 2020).

Another regional contrast showing higher R-pMn:R-pAl and R-pMn:R-pTi abundance in particles from the BENG region (1.88 and 62.1 mmol:mol, respectively; linear regression slope values), compared to NORTH (0.530 and 21.2 mmol:mol; linear regression slope values) was also apparent (Figure 6c), although the R-pMn abundances were deficient compared to average canonical UCC reference sources (4.67 and 176 mmol:mol, respectively; Rudnick & Gao, 2013) (Table S2 in Supporting Information S1). This feature was consistent with Mn deficiencies in Benguela sediment sources as reported by Böning et al. (2020).

In (near-)bottom waters of NORTH stations, the distributions of elevated lithogenic R-pTMs (Al, Ti, and Fe) were also largely consistent with benthic resuspension (Figure 4), with some evidence for lateral transport of benthic (nepheloid) particles off-shelf (Figure 6). Samples at intermediate depths with elevated R-pAl concentrations, observed at station 9 (400–800 m; 70–204 nM R-pAl), and between stations 17–19 (100–300 m; 20.5–25.2 nM R-pAl) (Figure 4), exhibited relatively consistent R-pFe:R-pAl and R-pAl:R-pTi ratios (Figure 6), reflecting nepheloid particles from the same respective (lithogenic) sources. The latter nepheloid layer source (100–300 m; ST 17–19) appeared to persist laterally off-shelf into the open ocean through stations 20 and 21 within isopycnal densities of the SACW (~26.3–26.9 kg $m^{-3}$ $\sigma_\Theta$), over 300 km away from the African shelf, as suggested by the relatively consistent sample R-pFe:R-pAl ratios (Figure 6). This illustrated the role of shelf particles as potential vectors onto which TMs may be carried off-shelf and into the Angola Dome, facilitated via adsorption directly onto lithogenic particles, or concomitantly with other co-occurring particle phases, such as (re-)precipitated Fe and Mn oxides (Burdige, 1993). Additionally, high particle concentrations, such as those in nepheloid layers, but also in river plume particles (ST 16–20), may facilitate enhanced scavenging (Honeyman et al., 1988; Rutgers Van Der Loeff & Boudreau, 1997), increasing the L-pTM pools of essential elements, such as Fe, subsequently buffering dTM pools (Achterberg et al., 2018; Milne et al., 2017). The role of advected

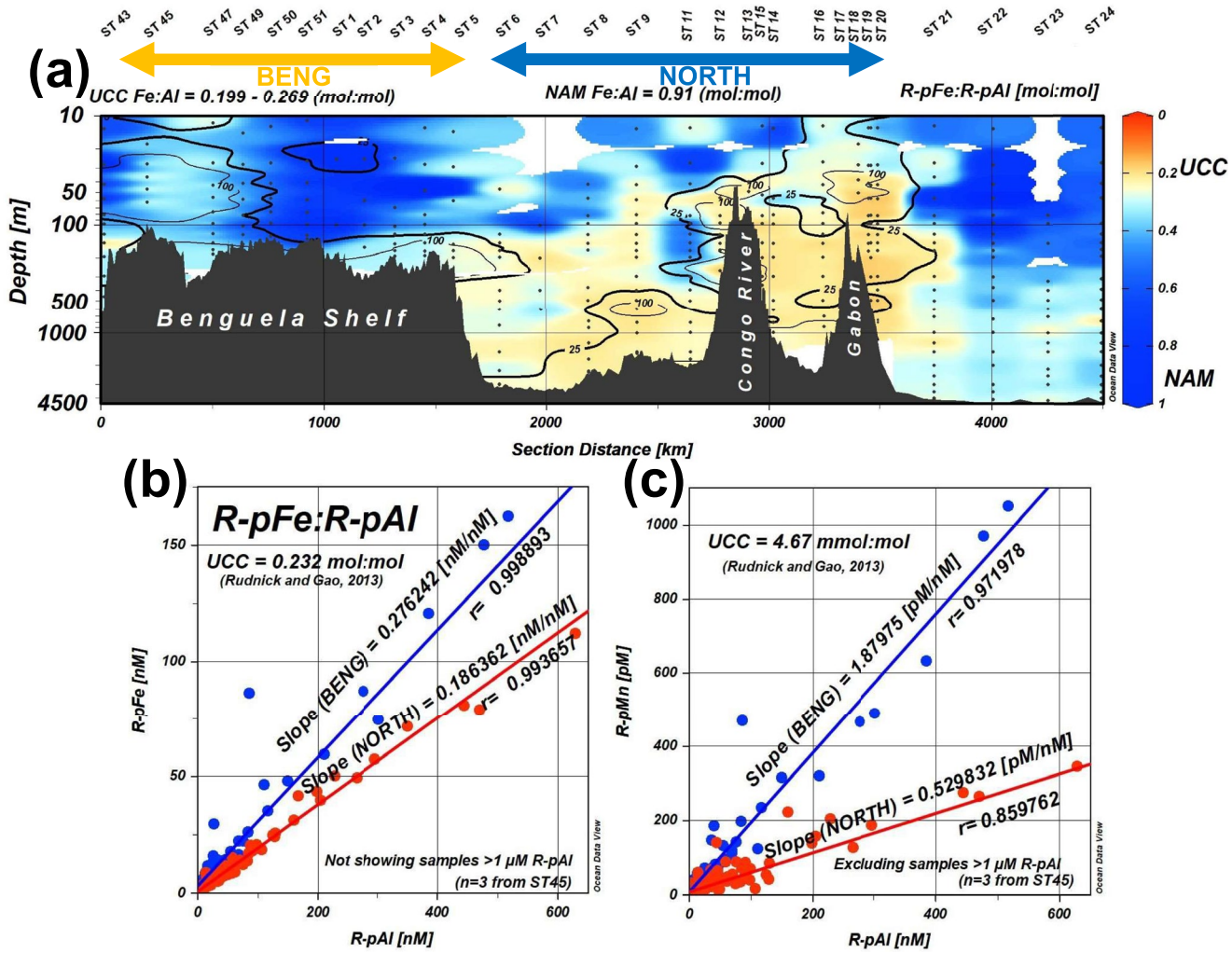


**Figure 6.** Spatial distribution of sample elemental ratios of refractory particulate iron (R-pFe) and aluminum (R-pAl) (a); and scatter plots illustrating regional contrasts in refractory particle compositions showing (b) enriched R-pFe abundance in BENG region (ST 43–51; and 1–5) compared to the NORTH (ST 6–24); and (c) refractory particulate Mn (R-pMn) abundance between BENG and NORTH regions. Note the logarithmic depth scale on (a). Reference elemental ratio ranges for Namibian desert dust (NAM) (Annegarn et al., 1983; Eltayeb et al., 1993) and Upper Continental Crust (UCC) (Rudnick & Gao, 2013) are shown above the section plot and annotated on $z$-axis color bar scale (a), and within each respective scatter plot (b) and (c). Annotated contour lines indicate R-pAl concentrations >25 nM and >100 nM. The blue and red sample points and regression lines represent samples from the BENG and NORTH regions, respectively. Three samples were not shown on scatter plots (ST 45; 1.2–4.9 µM R-pAl) that stretched the scales and decreased resolution.

particles in supplementing available Fe pools was described in the North Atlantic (Achterberg et al., 2018; Milne et al., 2017), Southern (van der Merwe et al., 2015) and Pacific (Lam & Bishop, 2008; Lam et al., 2006) Oceans and, hence, may also be an important source to the Angola Dome. L-pFe and R-pAl were closely correlated ($r = 0.91$; $p < 0.001$; Table S6 in Supporting Information S1), indicating that benthic particles could play an important role in sustaining the available Fe pool required by phytoplankton through L-pFe phases. This is relevant for Fe (Beghoura et al., 2019; Burdige & Komada, 2020), which is often limiting to primary production (Boyd & Ellwood, 2010; Moore et al., 2013), but was not in waters on and immediately off the shelf of the Angola Dome (as determined through field incubations conducted between approximately at ST 10 and 21) (Browning et al., 2017).

Particles collected nearest the Congo River outflow (ST 13–15), exhibited R-pTM:R-pAl linear regression slope values of 0.202 Fe:Al, 8.08 Fe:Ti, and 39.1 Al:Ti (Figures S15a–S15c in Supporting Information S1), which are comparable to UCC reference ranges (0.232, 8.77, and 37.7 (mol:mol), respectively) (Rudnick & Gao, 2013). However, particles were also deficient in R-pMn (0.641 R-pMn:R-pAl and 24.0 R-pMn:R-pTi [mmol:mol]; Figures S15d and S15e in Supporting Information S1) by about an order of magnitude compared

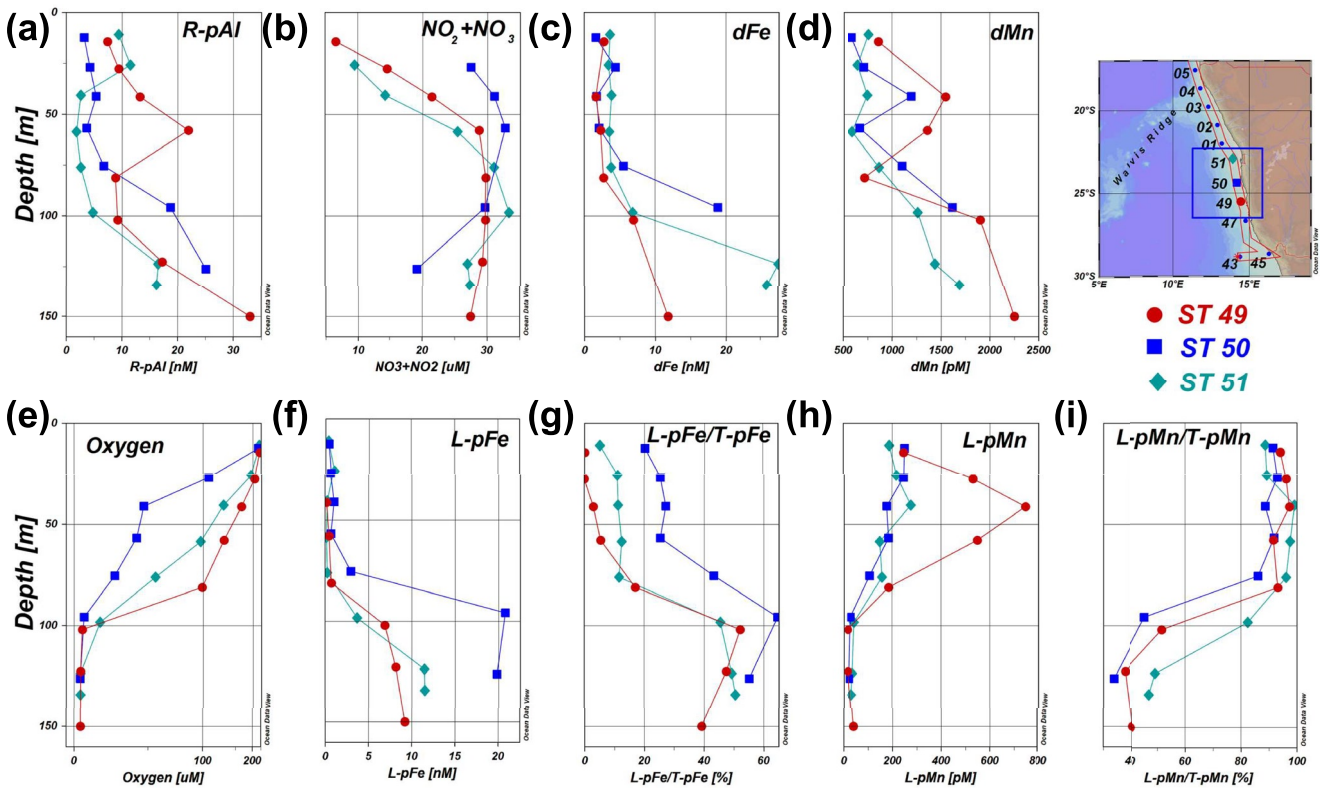


**Figure 7.** Water column profiles within the oxygen-depleted waters of the Lüderitz cell between stations 49–51 of (a) Refractory particulate aluminum (R-pAl); (b) Nitrate + Nitrite; (c) Dissolved Iron (dFe); (d) Dissolved Mn (dMn); (e) Dissolved Oxygen; (f) Labile particulate Fe (L-pFe); (g) Labile particulate Fe fraction (%); (h) Labile particulate Mn (L-pMn); (i) Labile particulate Mn fraction (%). Note the stretched scale for oxygen concentration.

to UCC reference values (4.67 R-pMn:R-pAl and 176 R-pMn:R-pTi, mmol:mol). No literature values reporting TM concentrations were available for Congo River particles to compare with our results at the time of this study. Particles in (sub-)surface waters with high lithogenic R-pTM in the river plume also exhibited increases in scavenging, particularly between stations 16–20, associated with high dTMs delivered by the river (Section 3.6).

Elevated L-pPb concentrations in benthic resuspended particles (R-pAl) were likely associated with anthropogenic Pb accumulated in sediments, which was released and subsequently (re-)adsorbed onto benthic particles following resuspension (Rusiecka et al., 2018). Re-adsorption of dissolved Pb may have occurred onto Fe and/or Mn oxides, or lithogenic particles (Chen, Goodkin, et al., 2016; Rusiecka et al., 2018; Rutgers Van Der Loeff & Boudreau, 1997), which is difficult to discern, as discussed in Section 3.3. However, the mechanism of Pb transport via resuspended benthic particles may be important for overall transfer of anthropogenic Pb from coastal to deeper ocean sediment inventories.

### 3.5. Iron and Manganese Cycling on the Benguela Shelf

The upwelling stations on the Benguela shelf were characterized by a more intense OMZ (<4 μM oxygen), compared to the Northern non-upwelling stations (>20 μM), and were underlain by anoxic and sulfidic sediments (Böning et al., 2020; Borchers et al., 2005; Inthorn et al., 2006). Stations 49–51 featured the most oxygen-deficient subsurface waters along the transect (<10 μM; 96–150 m; Figures 2b and 7e) and were located within the Lüderitz Cell.

In (near-)bottom waters at the NORTH stations with oxygen levels >20 μM (ST 6–20), L-pFe and L-pMn concentrations were enhanced, reaching up to 35.3 and 5.57 nM, respectively (Figure 3), coinciding with high lithogenic particle abundance (up to 469 nM R-pAl; Figure 4). The oxygen-depleted waters (<4 μM oxygen) on the Benguela shelf exhibited high L-pFe concentrations (up to 22.5 nM; ST 47–51 and 1–5), while L-pMn was comparatively low (18–357 pM; >75 m) (Figure 3). Vertical profiles for stations 49–51 featured increasing

concentrations of L-pFe (6.9–20.8 nM; Figure 7f) and dFe (11.8–27 nM; Figure 7c) below the oxycline toward the seafloor, where L-pFe comprised 39%–65% of the T-pFe pool (Figure 7g). In contrast, vertical L-pMn profiles showed decreasing concentrations (18.2–44.9 pM; Figure 7h) and L-pMn/T-pMn fractions with depth below the oxycline (34%–82% L-pMn/T-pMn; Figure 7i). Dissolved Fe and Mn concentrations (not shown) were enhanced in (near-)bottom waters where their labile particulate fractions were high, whilst dFe was particularly high on the Benguela Shelf (up to 27.4 nM; excluding ST 45, which was up to 46.3 nM) and dMn only slightly increasing with depth (1.27–2.25 nM Figure 7d). These differences in behavior of Fe and Mn were attributed to rapid oxidation kinetics of sediment derived Fe(II) and removal by precipitation (Elrod et al., 2004; Millero et al., 1987) and comparatively slower oxidation and further transport of Mn (Heggie & Lewis, 1984; Jensen et al., 2020; Klinkhammer, 1980; Luther et al., 2018; Tebo et al., 2004; 2005; von Langen et al., 1997).

The enhanced available Fe pools were associated with benthic supplies of reduced dFe(II) that rapidly precipitated as authigenic Fe oxides following oxidation by oxygen or nitrate, as observed in the oxycline of the Peruvian OMZ (Heller et al., 2017; Schlosser et al., 2018; Scholz et al., 2016) with subsequent accumulation in bottom waters and surface sediments. Nanoparticulate (colloidal [0.02–0.2 μm]) Fe oxides that may have precipitated (Raiswell & Canfield, 2012) are included in the operationally defined dFe pool (<0.2 μm), thus contributed to the enhanced dFe concentrations. Organically complexed Fe (Gledhill & Buck, 2012; Hopwood et al., 2020; Hunter & Boyd, 2007; Rue & Bruland, 1995; van den Berg, 1995), and non-reductive dissolution of lithogenic particles, as colloids (Homoky et al., 2013, 2021), may also supplement the dFe pool. The subsequent exchange of the colloidal Fe pool between the dissolved and particulate pools (i.e., through (dis-)aggregation) may explain the concomitant increase in both dFe and L-pFe fractions observed on the Benguela shelf (Boyd & Ellwood, 2010; Bruland & Lohan, 2003; Bruland et al., 2014) (Figures 7c and 7f).

The slight increase in dMn below the oxycline indicates a benthic source of reduced dMn (Burdige, 1993). The primarily microbially-mediated (bio-)oxidation of Mn (Moffett & Ho, 1996; Tebo et al., 2004, 2005; von Langen et al., 1997), was retarded in the oxygen-deficient environment, resulting in low L-pMn concentrations. Subsequent off-shelf transport of dMn in bottom seawater away from the shelf led to the relative depletion of Mn oxides within underlying sediment, consistent with regional sediment compositions reporting Mn depletion (Böning et al., 2020; Borchers et al., 2005).

However, poor correlations between L-pMn and L-pCo were observed in samples deeper than 50 m on the Benguela shelf ($r = 0.041$; ST 47–51 and 1–5; >50 m; Figure S16 in Supporting Information S1), with increases in L-pCo concentrations, relative to L-pMn, below the oxycline, indicating an additional source for L-pCo. This was ascribed to biogenic particles, driven by the increased production and longer remineralization length scales within the upwelling stations (Section 3.3). Also, pCo: pP ratios were relatively consistent (0.214 ± 0.186 and 0.243 ± 0.187 mmol:mol T-pCo:T-pP and L-pCo:L-pP, respectively; ST47-51 and 1–5) and generally in agreement with reported plankton stoichiometry ranges (Table 1).

Overall, the relative deficiency in Mn oxide production on the shelf, an important dCo sink (Hawco et al., 2018), may have been an important factor allowing enhanced dCo signals to be carried further off-shore within the OMZ and into the South Atlantic Ocean. This would provide an explanation for the dCo plume that was detected within the OMZ of the South Atlantic on the CoFeMUG (GAc01) transect (Noble et al., 2012, 2017), as the existence of an off-shore plume of dCo downstream within the open-ocean OMZ of the eastern tropical Pacific also relied on low concentrations of Mn oxides (Lam et al., 2018; Landing & Bruland, 1987; Lee et al., 2018; and Vedamati et al., 2015).

### 3.6. Congo River Plume

Samples collected in the Congo River plume (ST 13–20) exhibited patterns of enhanced TM adsorption that were associated with a high supply of dTMs by the river, combined with high particle abundance providing sites for adsorption. This was evident through increased L-pTM concentrations (Figure 3) and L-pTM/T-pTM fractions (Figure 5) coinciding with relatively high concentrations of R-pAl (57.6 ± 95.8 nM; ST 13–20) and T-pP at the surface (up to 47.0 nM; <100 m; ST 13–20). Enhanced dTM concentrations were measured in surface waters of the plume (~5 m, towed-fish samples), reaching up to 1.24 μM dFe, 784 nM dAl, 125 nM dMn, 1.04 nM dCo, 84 nM dPb, 8.13 nM dCu, 2.72 nM dZn, and 7.08 nM dNi (Figure S17 in Supporting Information S1; only dFe shown; other TMs will be presented elsewhere). The enhanced supply of TMs by the Congo River is likely

related to the presence of ore bodies and copper-cobalt mining in the Congo catchment (Prasad, 1989). Enhanced particle-reactive L-pTM (notably Fe, Mn, Al, and Pb) concentrations and L-pTM/T-pTM ratios were observed at the coastal plume stations (ST 12–20), reaching up to 22.6 nM (64.8%) L-pFe, 2.3 nM (99.4%) L-pMn, 21.6 nM (77.5%) L-pAl, and 14.3 pM (93.2%) L-pPb (Figures 3 and 5). Dissolved Fe was particularly enhanced within TSW (up to 8.75 nM; <20 m) and persisted north of the river mouth and westward into the open ocean through to station 22 (3.69 nM at ST 22) (not shown). However, enhanced L-pFe concentrations (up to 34.9 nM) were mostly confined to the coastal plume stations (ST 13–20) and were relatively low within TSW off-shelf (mean 0.136 ± 0.125 nM L-pFe at ST 21–22; ≤100 m; $n$ = 12). Similarly, L-pAl and L-pPb concentrations were enhanced in surface waters of the coastal plume stations (up to 21.6 nM and 11.3 pM, respectively; ST 12–20; <50 m; Figure 3) and did not persist off-shelf. In contrast, enhanced L-pMn concentrations (up to 3.51 nM; ST 12–20) were relatively persistent off-shelf within TSW (617 pM L-pMn at ST 22) and coincided with elevated dMn (up to 6.47 nM at ST 13; and 4.87 nM dMn at ST 22) in river plume stations. Elevated dMn concentrations also persisted within STUW south of the Congo River mouth (3.21 ± 0.93 nM dMn; ST 8–11; <50 m; $n$ = 7; not shown) and coincided with low L-pMn concentrations (177 ± 118 pM; ST 8–11; <50 m; $n$ = 7) (Figure 3).

In agreement with the dissolved and labile pTM observations, available Fe, Mn, and Al at the coastal plume stations (ST 13–20) were enhanced with concentrations up to 41.3, 7.23, and 104 nM, respectively (Figures S18e–S18g in Supporting Information S1). The available Pb concentrations were not enhanced and were higher on the Benguela shelf. Enhanced available Mn and Al concentrations that were associated with the river plume persisted off-shelf within TSW as far west as ST 22, and possibly southward as well for Mn (ST 8–11) (Figures S18f and S18g in Supporting Information S1). Available Fe and Pb, did not persist off-shelf (Figures S18e and S18h in Supporting Information S1). The enhanced available Al pool in plume samples was dominated by dAl, which were high (up to 85 nM dAl, and 98% of available Al), while L-pAl was relatively low off-shelf (Figure S18g in Supporting Information S1). In contrast, L-pFe comprised most of the available Fe pool in coastal plume stations (up to 93%) but was also low off-shelf. The low L-pFe and L-pAl concentrations off-shelf implied that particles played a decreasing role in sustaining elevated dFe and dAl concentrations off-shelf, which were instead sustained through other mechanisms. Dissolved Fe is likely kept in solution by complexation with organic ligands (Buck et al., 2015; Gledhill & Buck, 2012; Hopwood et al., 2020; Hunter & Boyd, 2007; van den Berg, 1995) and also photo- and/or non-reductive dissolution processes from lithogenic particles (Homoky et al., 2013, 2021). The latter case may also support the explanation of the persistently elevated dAl signal within the plume.

Increased L-pTM/dTM fractions of Fe, Mn, and Pb were evident in the coastal plume (sub-)surface waters, consistent with increased adsorption and/or precipitation of labile Fe and Mn oxides (Figures S18a, S18b, and S18d in Supporting Information S1), compared to non-plume stations. Lithogenic particle concentrations were also enhanced, particularly between stations 16–20 (up to 628 nM R-pAl). Increases in L-pTM/dTM partitioning of Pb, Fe and Mn were co-distributed with R-pAl, suggesting that lithogenic particles were important sites for adsorption, including Fe and Mn oxides. Closer correlations of L-pPb and L-pAl with L-pFe ($r$ = 0.919 and 0.691, respectively; Figures S19a and 19b in Supporting Information S1) over L-pMn ($r$ = 0.787 and 0.529, respectively; Figures S19c and 19d in Supporting Information S1) may suggest a slight preferential affinity for Al and Pb with Fe oxides, or that they shared preferential affinities to same particle surfaces as Fe. Although, the closer correlations to L-pFe may be due to a comparatively higher abundance of labile Fe oxides, compared to Mn oxides, and corresponding binding sites for adsorption.

Elevated L-pMn, persisted in photic surface waters, within the TSW (<25 m), away from the shelf (to ST 22), in contrast to L-pFe and L-pPb. This suggested that either Mn had an increased affinity for particles at the surface (i.e., biogenic particles) or that Fe and Pb had a steeper removal gradient than Mn toward off-shelf waters. T-pMn:T-pP (17 and 26 mmol:mol; ST 21 and 22, respectively; $n$ = 2) and L-pMn:L-pP (116 and 97 mmol:mol; ST 21 and 22, respectively; $n$ = 2) ratios were higher than reported biogenic particle stoichiometries (Table 1), and Mn oxides abundance in surface waters are decreased due to photo-reductive dissolution (Sunda & Huntsman, 1988, 1994). This left biogenic particles as the dominant particulate phases in offshore surface waters (ST21-22; <25 m) onto which dissolved Mn may adsorb onto, although this assumption is based on only a few datapoints.

The adsorptive processes occurring within the plume indicated that adsorbed pFe (i.e., L-pFe) likely played an important role in maintaining elevated dFe concentrations in coastal plume stations (ST 13–20) through reversible adsorption (Achterberg et al., 2018, 2021; Milne et al., 2017), with a lower influence in off-shelf plume waters (within TSW in ST 21 and 22). However, it was also apparent that reversible-scavenging was either not in

equilibrium and/or that variable supplies of dFe may have occurred in the shelf waters, as L-pFe and dFe showed a weak correlation ($r = 0.2718$; ST 13–20; $n = 70$).

## 4. Conclusions

Overall, this work provides important insights to the biogeochemical cycling processes and the influences of different environments controlling pTM distributions in the southwest African shelf and the Angola basin region. Our results complement regional studies of shelf sediments by providing a snapshot of processes occurring in the overlying water column and illustrate a decoupled redox cycling of Fe and Mn on the Benguela shelf, with Fe retention and Mn transport off-shelf. Additionally, we illustrate several advantages of how separating the labile from refractory particulate fractions may be utilized to enhance the interpretations of pTM cycling, though also highlight some cautions and potential considerations for future work as well.

The decoupled distributions of Fe oxide enrichment and Mn oxide deficiency in the oxygen-depleted waters on the Benguela shelf could have broader implications on TM cycling and export in other upwelling regions of the ocean. Iron oxides precipitated and accumulated in bottom waters are a potential source of Fe following subsequent transport. In cases where seasonal oxygen depletion occurs, subsequent advection of bottom waters may supply a source of available Fe (and associated scavenged TMs) downstream that may potentially support or enhance primary production. Manganese oxide deficiency under sub-oxic conditions could enhance the shuttling of typically associated TMs, such as Co, away from the shelf. Indeed, the transport of Co to the South Atlantic Ocean appears to be facilitated by enhanced supply from benthic sources on the oxygen-depleted Benguela shelf.

The Congo River plume formed a significant source of available TMs to the shelf, mainly through enhanced scavenging, reflected in labile pTM fractions, with subsequent buffering of dTM concentrations in shelf and off-shelf waters. However, the role of plume particles in sustaining dTM concentrations off-shelf did not appear to be dominant. Transport of available Fe within the river plume was instead sustained within the dissolved fraction, likely following the photo-reductive release of Fe(II) from lithogenic particles and/or ligand-bound dFe. However, dissolved Mn removal from the water column through scavenging appeared less efficient than dFe, allowing it to persist off-shelf.

Bio-essential pTM:pP ratios (Zn, Ni, Cd, Co, and Cu) of labile and total particulate fractions in surface waters were comparable to reported plankton stoichiometries, implying the predominant association of their pTM pools with biogenic particles. However, labile particulate Fe and Mn pools in surface waters included a significant fraction of L-pTM phases attributed to adsorption onto cell surfaces and also the possible inclusion of labile Fe and Mn oxides. Additionally, the variability in labile biogenic particle fractions, in particular for pP, highlighted the need to exercise caution when interpreting labile fractions, importantly when comparing pTM data sets between ocean basins and across seasons.

The relatively high refractory biogenic pP fractions observed across several stations raises some uncertainties that require further investigation in future work, specifically into the chemical lability of major phytoplankton taxa groups when applying chemical leaches. With the increased adoption of the Berger et al. (2008) leach, as its use is recommended in GEOTRACES standard protocols (i.e., the GEOTRACES "Cookbook"; Cutter et al., 2017), further improvement of biogenic particle characterization will improve inter-comparison of pTM cycling in other regions, enhancing pTM cycling components in biogeochemical modeling, and providing relevant insights for paleoceanographic and benthic interpretations as well.

The observations and conclusions in this work contribute to a growing body of literature (e.g., Lee et al., 2018; Lippiatt, Brown, et al., 2010; Milne et al., 2017; Twining et al., 2019; Xiang & Lam, 2020) demonstrating the importance of particles for TM cycling and transport within the ocean and emphasize the importance of selective leach procedures for understanding TM cycling by particles.

## Conflict of Interest

The authors declare no conflicts of interest relevant to this study.

## Data Availability Statement

The full data sets for labile (L-pTM), refractory (R-pTM), and total (T-pTM) particulate trace metal concentrations of Iron (Fe), Aluminum (Al), Titanium (Ti), Manganese (Mn), Cobalt (Co), Zinc (Zn), Nickel (Ni), Copper (Cu), Cadmium (Cd), and Lead (Pb), and particulate Phosphorus (P) for the presented sections of the GA08 (M121) cruise transect are available at https://doi.pangaea.de/10.1594/PANGAEA.945498 (Al-Hashem et al., 2022). The full data set for dissolved TM (dTM) concentrations of Fe, Co, Mn, Ni, Cd, Cu, Pb and Zn, Fe(II), and macronutrients (phosphate, nitrate + nitrite, and silicic acid) concentrations are available at https://doi.org/10.1594/PANGAEA.947275 (Liu et al., 2022). The data set for the presented sections of the GA08 (M121) cruise transect are also provided as a Source Data file.

**Acknowledgments**

We thank the captain and crew of the RV Meteor M121 cruise/GEOTRACES GA08 section; S. Koesling, P. Lodeiro, J. Pampín Baro, J. C. Yong and C. Schlosser for cruise support and assistance in sample collection and P. Streu and Bernhard Wenzel for technical laboratory assistance. Detailed comments by an anonymous reviewer improved the manuscript who is gratefully acknowledged. The PhD fellowships to A. Al-Hashem and S. Krisch were funded by the Kuwait Institute for Scientific Research, Kuwait, and the Deutsche Forschungsgemeinschaft (AC 217/1-1 granted to Eric P. Achterberg), respectively. The cruise was funded by the Deutsche Forschungsgemeinschaft (DFG). The open-access publishing charges for this publication were covered by the Helmholtz Research Centre/Association. The GEOTRACES 2021 Intermediate Data Product (IDP2021) represents an international collaboration and is endorsed by the Scientific Committee on Oceanic Research (SCOR). The many researchers and funding agencies responsible for the collection of data and quality control are thanked for their contributions to the IDP2021. Open Access funding enabled and organized by Projekt DEAL.

## References

Achterberg, E. P., Holland, T. W., Bowie, A. R., Mantoura, R. F. C., & Worsfold, P. J. (2001). Determination of iron in seawater. *Analytica Chimica Acta*, *442*(1), 1–14. https://doi.org/10.1016/S0003-2670(01)01091-1

Achterberg, E. P., Steigenberger, S., Klar, J. K., Browning, T. J., Marsay, C. M., Painter, S. C., et al. (2021). Trace element biogeochemistry in the high-latitude North Atlantic Ocean: Seasonal variations and volcanic inputs. *Global Biogeochemical Cycles*, *35*(3), e2020GB006674. https://doi.org/10.1029/2020GB006674

Achterberg, E. P., Steigenberger, S., Marsay, C. M., Lemoigne, F. A. C., Painter, S. C., Baker, A. R., et al. (2018). Iron biogeochemistry in the high latitude North Atlantic Ocean. *Scientific Reports*, *8*(1), 1283. https://doi.org/10.1038/s41598-018-19472-1

Al-Hashem, A. A., Beck, A., & Achterberg, E. P. (2022). Labile, refractory, and total particulate trace metal concentrations from the GEOTRACES GA08 shelf section and 3-degree latitudinal transect. PANGAEA. https://doi.org/10.1594/PANGAEA.945498

Allen, J. R. L., Rae, J. E., & Zanin, P. E. (1990). Metal speciation (Cu, Zn, Pb) and organic matter in an oxic salt marsh, Severn Estuary, southwest Britain. *Marine Pollution Bulletin*, *21*(12), 574–580. https://doi.org/10.1016/0025-326X(90)90606-9

Anderson, R. F. (2020). GEOTRACES: Accelerating research on the marine biogeochemical cycles of trace elements and their isotopes. *Annual Review of Marine Science*, *12*(1), 49–85. https://doi.org/10.1146/annurev-marine-010318-095123

Annegarn, H. J., van Grieken, R. E., Bibby, D. M., & von Blottnitz, F. (1983). Background aerosol composition in the namib desert, South West Africa (Namibia). *Atmospheric Environment*, *17*(10), 2045–2053. https://doi.org/10.1016/0004-6981(83)90361-X

Archer, C., Vance, D., Milne, A., & Lohan, M. C. (2020). The oceanic biogeochemistry of nickel and its isotopes: New data from the South Atlantic and the Southern Ocean biogeochemical divide. *Earth and Planetary Science Letters*, *535*, 116118. https://doi.org/10.1016/j.epsl.2020.116118

Armstrong, R. A., Lee, C., Hedges, J. I., Honjo, S., & Wakeham, S. G. (2001). A new, mechanistic model for organic carbon fluxes in the ocean based on the quantitative association of POC with ballast minerals. *Deep-Sea Research Part II Topical Studies in Oceanography*, *49*(1–3), 219–236. https://doi.org/10.1016/S0967-0645(01)00101-1

Barrett, P. M., Resing, J. A., Grand, M. M., Measures, C. I., & Landing, W. M. (2018). Trace element composition of suspended particulate matter along three meridional CLIVAR sections in the Indian and Southern Oceans: Impact of scavenging on Al distributions. *Chemical Geology*, *502*, 15–28. https://doi.org/10.1016/j.chemgeo.2018.06.015

Beghoura, H., Gorgues, T., Aumont, O., Planquette, H., Tagliabue, A., & Auger, P. A. (2019). Impact of inorganic particles of sedimentary origin on global dissolved iron and phytoplankton distribution. *Journal of Geophysical Research: Oceans*, *124*(12), 8626–8646. https://doi.org/10.1029/2019JC015119

Berger, C. J. M., Lippiatt, S. M., Lawrence, M. G., & Bruland, K. W. (2008). Application of a chemical leach technique for estimating labile particulate aluminum, iron, and manganese in the Columbia River plume and coastal waters off Oregon and Washington. *Journal of Geophysical Research*, *113*, 1–16. https://doi.org/10.1029/2007JC004703

Bianchi, D., Weber, T. S., Kiko, R., & Deutsch, C. (2018). Global niche of marine anaerobic metabolisms expanded by particle microenvironments. *Nature Geoscience*, *11*(4), 263–268. https://doi.org/10.1038/s41561-018-0081-0

Birchill, A. J., Milne, A., Woodward, E. M. S., Harris, C., Annett, A. L., Rusiecka, D., et al. (2017). Seasonal iron depletion in temperate shelf seas. *Geophysical Research Letters*, *44*(17), 8987–8996. https://doi.org/10.1002/2017GL073881

Bishop, J. K. B., Wood, T. J., Davis, R. E., & Sherman, J. T. (2004). Robotic observations of enhanced carbon biomass and export at 55°S during SOFeX. *Science*, *304*(5669), 417–420. https://doi.org/10.1126/science.1087717

Böning, P., Schnetger, B., Belz, L., Ferdelman, T. G., Brumsack, H. J., & Pahnke, K. (2020). Sedimentary iron cycling in the Benguela upwelling system off Namibia. *Earth and Planetary Science Letters*, *538*, 116212. https://doi.org/10.1016/j.epsl.2020.116212

Borchers, S. L., Schnetger, B., Böning, P., & Brumsack, H. J. (2005). Geochemical signatures of the Namibian diatom belt: Perennial upwelling and intermittent anoxia. *Geochemistry, Geophysics, Geosystems*, *6*(6), Q06006. https://doi.org/10.1029/2004GC000886

Boyd, P. W., & Ellwood, M. J. (2010). The biogeochemical cycle of iron in the ocean. *Nature Geoscience*, *3*(10), 675–682. https://doi.org/10.1038/ngeo964

Boyd, P. W., Ellwood, M. J., Tagliabue, A., & Twining, B. S. (2017). Biotic and abiotic retention, recycling and remineralization of metals in the ocean. *Nature Geoscience*, *10*(3), 167–173. https://doi.org/10.1038/ngeo2876

Boyle, E. A., Bergquist, B. A., Kayser, R. A., & Mahowald, N. M. (2005). Iron, manganese, and lead at Hawaii Ocean Time-series station ALOHA: Temporal variability and an intermediate water hydrothermal plume. *Geochimica et Cosmochimica Acta*, *69*(4), 933–952. https://doi.org/10.1016/J.GCA.2004.07.034

Boyle, E. A., Sclater, F. R., & Edmond, J. M. (1977). The distribution of dissolved copper in the Pacific. *Earth and Planetary Science Letters*, *37*(1), 38–54. https://doi.org/10.1016/0012-821X(77)90144-3

Bremner, J. M., & Willis, J. P. (1993). Mineralogy and geochemistry of the clay fraction of sediments from the Namibian continental margin and the adjacent hinterland. *Marine Geology*, *115*(1–2), 85–116. https://doi.org/10.1016/0025-3227(93)90076-8

Browning, T. J., Achterberg, E. P., Engel, A., & Mawji, E. (2021). Manganese co-limitation of phytoplankton growth and major nutrient drawdown in the Southern Ocean. *Nature Communications*, *12*(1), 1–9. https://doi.org/10.1038/s41467-021-21122-6

Browning, T. J., Achterberg, E. P., Rapp, I., Engel, A., Bertrand, E. M., Tagliabue, A., & Moore, C. M. (2017). Nutrient co-limitation at the boundary of an oceanic gyre. *Nature*, *551*(7679), 242–246. https://doi.org/10.1038/nature24063

Bruland, K. W. (1980). Oceanographic distributions of cadmium, zinc, nickel, and copper in the North Pacific. *Earth and Planetary Science Letters*, *47*(2), 176–198. https://doi.org/10.1016/0012-821X(80)90035-7

Bruland, K. W., & Lohan, M. C. (2003). Controls of trace metals in Seawater. *The Oceans and Marine Geochemistry*, *6*, 23–47.
Bruland, K. W., Middag, R., & Lohan, M. C. (2014). *Controls of trace metals in seawater. Treatise on geochemistry*, 2nd ed. (Vol. 8). Elsevier Ltd. https://doi.org/10.1016/B978-0-08-095975-7.00602-1
Buck, K. N., Sohst, B., & Sedwick, P. N. (2015). The organic complexation of dissolved iron along the U.S. GEOTRACES (GA03) North Atlantic Section. *Deep-Sea Research Part II Topical Studies in Oceanography*, *116*, 152–165. https://doi.org/10.1016/j.dsr2.2014.11.016
Burdige, D. J. (1993). The biogeochemistry of manganese and iron reduction in marine sediments. *Earth-Science Reviews*, *35*(3), 249–284. https://doi.org/10.1016/0012-8252(93)90040-E
Burdige, D. J., & Komada, T. (2020). Iron redox cycling, sediment resuspension and the role of sediments in low oxygen environments as sources of iron to the water column. *Marine Chemistry*, *223*(September 2019), 103793. https://doi.org/10.1016/j.marchem.2020.103793
Carr, M. E. (2001). Estimation of potential productivity in Eastern Boundary Currents using remote sensing. *Deep Sea Research Part II: Topical Studies in Oceanography*, *49*(1–3), 59–80. https://doi.org/10.1016/S0967-0645(01)00094-7
Charette, M. A., Lam, P. J., Lohan, M. C., Kwon, E. Y., Hatje, V., Jeandel, C., et al. (2016). Coastal ocean and shelf-sea biogeochemical cycling of trace elements and isotopes: Lessons learned from GEOTRACES. *Philosophical Transactions of the Royal Society A: Mathematical, Physical & Engineering Sciences*, *374*(2081), 20160076. https://doi.org/10.1098/rsta.2016.0076
Chen, M., Boyle, E. A., Lee, J. M., Nurhati, I., Zurbrick, C., Switzer, A. D., & Carrasco, G. (2016). Lead isotope exchange between dissolved and fluvial particulate matter: A laboratory study from the Johor river estuary. *Philosophical Transactions of the Royal Society A: Mathematical, Physical & Engineering Sciences*, *374*(2081), 20160054. https://doi.org/10.1098/rsta.2016.0054
Chen, M., Goodkin, N. F., Boyle, E. A., Switzer, A. D., & Bolton, A. (2016). Lead in the western South China Sea: Evidence of atmospheric deposition and upwelling. *Geophysical Research Letters*, *43*(9), 4490–4499. https://doi.org/10.1002/2016GL068697
Chuang, C. Y., Santschi, P. H., Jiang, Y., Ho, Y. F., Quigg, A., Guo, L., et al. (2014). Important role of biomolecules from diatoms in the scavenging of particle-reactive radionuclides of thorium, protactinium, lead, polonium, and beryllium in the ocean: A case study with Phaeodactylum tricornutum. *Limnology & Oceanography*, *59*(4), 1256–1266. https://doi.org/10.4319/LO.2014.59.4.1256
Cochran, J. K., McKibbin-Vaughan, T., Dornblaser, M. M., Hirschberg, D., Livingston, H. D., & Buesseler, K. O. (1990). 210Pb scavenging in the North Atlantic and North Pacific oceans. *Earth and Planetary Science Letters*, *97*(3–4), 332–352. https://doi.org/10.1016/0012-821X(90)90050-8
Collier, R., & Edmond, J. (1984). The trace element geochemistry of marine biogenic particulate matter. *Progress in Oceanography*, *13*(2), 113–199. https://doi.org/10.1016/0079-6611(84)90008-9
Compton, J. S., & Bergh, E. W. (2016). Phosphorite deposits on the Namibian shelf. *Marine Geology*, *380*, 290–314. https://doi.org/10.1016/j.margeo.2016.04.006
Cowen, J. P., & Bruland, K. W. (1985). Metal deposits associated with bacteria: Implications for Fe and Mn marine biogeochemistry. *Deep-Sea Research, Part A: Oceanographic Research Papers*, *32*(3), 253–272. https://doi.org/10.1016/0198-0149(85)90078-0
Cullen, J. T., Chase, Z., Coale, K. H., Fitzwater, S. E., & Sherrell, R. M. (2003). Effect of iron limitation on the cadmium to phosphorus ratio of natural phytoplankton assemblages from the Southern Ocean. *Limnology & Oceanography*, *48*(3), 1079–1087. https://doi.org/10.4319/LO.2003.48.3.1079
Cullen, J. T., Field, M. P., & Sherrell, R. M. (2001). Determination of trace elements in filtered suspended marine particulate material by sector field HR-ICP-MS. *The Royal Society of Chemistry*, *16*, 1307–1312. https://doi.org/10.1039/b104398f
Cullen, J. T., & Sherrell, R. M. (1999). Techniques for determination of trace metals in small samples of size-fractionated particulate matter: Phytoplankton metals off central California. *Marine Chemistry*, *67*(3–4), 233–247. https://doi.org/10.1016/s0304-4203(99)00060-2
Cutter, G. A., Andersson, P. S., Codispoti, L., Croot, P. L., Francois, R., Lohan, M. C., et al. (2010). Sampling and sample-handling protocols for GEOTRACES cruises (pp. 1–238). Retrieved from http://www.geotraces.org/science/intercalibration/222-sampling-and-sample-handling-protocols-for-geotraces-cruises
Cutter, G. A., Casciotti, K., Croot, P. L., Geibert, W., Heimbürger, L.-E., Lohan, M. C., et al. (2017). Sampling and sample-handling protocols for GEOTRACES Cruises. Version 3, August 2017. GEOTRACES Community practices & Appendices (p. 139). Retrieved from http://www.geotraces.org/images/stories/documents/intercalibration/Cookbook.pdf
Elrod, V. A., Berelson, W. M., Coale, K. H., & Johnson, K. S. (2004). The flux of iron from continental shelf sediments: A missing source for global budgets. *Geophysical Research Letters*, *31*(12), L12307. https://doi.org/10.1029/2004gl020216
Eltayeb, M. A. H., van Grieken, R. E., Maenhaut, W., & Annegarn, H. J. (1993). Aerosol-soil fractionation for Namib Desert samples. *Atmospheric Environment, Part A: General Topics*, *27*(5), 669–678. https://doi.org/10.1016/0960-1686(93)90185-2
Fernex, F., Février, G., Bénaïm, J., & Arnoux, A. (1992). Copper, lead and zinc trapping in mediterranean deep-sea sediments: Probable coprecipitation with Mn and Fe. *Chemical Geology*, *98*(3–4), 293–306. https://doi.org/10.1016/0009-2541(92)90190-G
Gledhill, M., & Buck, K. N. (2012). The organic complexation of iron in the marine environment: A review. *Frontiers in Microbiology*, *3*(February), 1–17. https://doi.org/10.3389/fmicb.2012.00069
Goldberg, E. D. (1954). Chemical scavengers of the sea. *The Journal of Geology*, *62*(3), 249–265. https://doi.org/10.1086/626161
Govin, A., Holzwarth, U., Heslop, D., Ford Keeling, L., Zabel, M., Mulitza, S., et al. (2012). Distribution of major elements in Atlantic surface sediments (36°N–49°S): Imprint of terrigenous input and continental weathering. *Geochemistry, Geophysics, Geosystems*, *13*(1), 1–23. https://doi.org/10.1029/2011GC003785
Hansen, H. P. (2007). Determination of oxygen. Methods of seawater analysis: Third, completely revised and extended edition (pp. 75–89). https://doi.org/10.1002/9783527613984.CH4
Hawco, N. J., Lam, P. J., Lee, J. M., Ohnemus, D. C., Noble, A. E., Wyatt, N. J., et al. (2018). Cobalt scavenging in the mesopelagic ocean and its influence on global mass balance: Synthesizing water column and sedimentary fluxes. *Marine Chemistry*, *201*, 151–166. https://doi.org/10.1016/j.marchem.2017.09.001
Heggie, D., & Lewis, T. (1984). Cobalt in pore waters of marine sediments. *Nature*, *311*(5985), 453–455. https://doi.org/10.1038/311453a0
Heller, M. I., Lam, P. J., Moffett, J. W., Till, C. P., Lee, J.-M., Toner, B. M., & Marcus, M. A. (2017). Accumulation of Fe oxyhydroxides in the Peruvian oxygen deficient zone implies non-oxygen dependent Fe oxidation. *Geochimica et Cosmochimica Acta*, *211*, 174–193. https://doi.org/10.1016/j.gca.2017.05.019
Henderson, G. M., & Marchal, O. (2015). Recommendations for future measurement and modelling of particles in GEOTRACES and other ocean biogeochemistry programmes. *Progress in Oceanography*, *133*, 73–78. https://doi.org/10.1016/j.pocean.2015.01.015
Ho, T.-Y., Finkel, Z. V., Milligan, A. J., Wyman, K., Falkowski, P. G., & Morel, F. M. M. (2003). The elemental composition of some marine phytoplankton. *Journal of Phycology*, *39*(6), 1145–1159. https://doi.org/10.1111/j.0022-3646.2003.03-090.x
Homoky, W. B., Conway, T. M., John, S. G., König, D., Deng, F. F., Tagliabue, A., & Mills, R. A. (2021). Iron colloids dominate sedimentary supply to the ocean interior. *Proceedings of the National Academy of Sciences of the United States of America*, *118*(13), e2016078118. https://doi.org/10.1073/PNAS.2016078118

Homoky, W. B., John, S. G., Conway, T. M., & Mills, R. A. (2013). Distinct iron isotopic signatures and supply from marine sediment dissolution. *Nature Communications*, *4*, 1–2. https://doi.org/10.1038/ncomms3143

Honeyman, B. D., Balistrieri, L. S., & Murray, J. W. (1988). Oceanic trace metal scavenging: The importance of particle concentration. *Deep-Sea Research, Part A: Oceanographic Research Papers*, *35*(2), 227–246. https://doi.org/10.1016/0198-0149(88)90038-6

Hopwood, M. J., Santana-González, C., Gallego-Urrea, J., Sanchez, N., Achterberg, E. P., Ardelan, M. V., et al. (2020). Fe(II) stability in coastal seawater during experiments in Patagonia, Svalbard, and Gran Canaria. *Biogeosciences*, *17*(5), 1327–1342. https://doi.org/10.5194/bg-17-1327-2020

Hunter, K. A., & Boyd, P. W. (2007). Iron-binding ligands and their role in the ocean biogeochemistry of iron. *Environmental Chemistry*, *4*(4), 221–232. https://doi.org/10.1071/EN07012

Hurst, M. P., Aguliar-Islas, A., & Bruland, K. W. (2010). Iron in the southeastern Bering Sea: Elevated leachable particulate Fe in shelf bottom waters as an important source for surface waters. *Continental Shelf Research*, *30*(5), 467–480. https://doi.org/10.1016/j.csr.2010.01.001

Hurst, M. P., & Bruland, K. W. (2008). The effects of the San Francisco Bay plume on trace metal and nutrient distributions in the Gulf of the Farallones. *Geochimica et Cosmochimica Acta*, *72*(2), 395–411. https://doi.org/10.1016/j.gca.2007.11.005

Hydes, D. J., & Liss, P. S. (1976). Fluorimetric method for the determination of low concentrations of dissolved aluminium in natural waters. *Analyst*, *101*(1209), 922–931. https://doi.org/10.1039/AN9760100922

Inthorn, M., Mohrholz, V., & Zabel, M. (2006). Nepheloid layer distribution in the Benguela upwelling area offshore Namibia. *Deep-Sea Research Part I Oceanographic Research Papers*, *53*(8), 1423–1438. https://doi.org/10.1016/j.dsr.2006.06.004

Jeandel, C., Rutgers van der Loeff, M., Lam, P. J., Roy-Barman, M., Sherrell, R. M., Kretschmer, S., et al. (2015). What did we learn about ocean particle dynamics in the GEOSECS-JGOFS era? *Progress in Oceanography*, *133*, 6–16. https://doi.org/10.1016/j.pocean.2014.12.018

Jensen, L. T., Morton, P. L., Twining, B. S., Heller, M. I., Hatta, M., Measures, C. I., et al. (2020). A comparison of marine Fe and Mn cycling: U.S. GEOTRACES GN01 Western Arctic case study. *Geochimica et Cosmochimica Acta*, *288*, 138–160. https://doi.org/10.1016/j.gca.2020.08.006

Jian-rui, W., & Jie, Z. (2016). Study on the selective leaching of low-grade phosphate ore for beneficiation of phosphorus and rare earths using citric acid as leaching agent. *Russian Journal of Applied Chemistry*, *89*(7), 1196–1205. https://doi.org/10.1134/S1070427216070211

Jickells, T. D., An, Z. S., Andersen, K. K., Baker, A. R., Bergametti, G., Brooks, N., et al. (2005). Global iron connections between desert dust, ocean biogeochemistry, and climate. *Science*, *308*(5718), 67–71. https://doi.org/10.1126/science.1105959

Klaas, C., & Archer, D. E. (2002). Association of sinking organic matter with various types of mineral ballast in the deep sea: Implications for the rain ratio. *Global Biogeochemical Cycles*, *16*(4), 63-1–63-14. https://doi.org/10.1029/2001gb001765

Klein, N. J., Beck, A. J., Hutchins, D. A., & Sañudo-Wilhelmy, S. A. (2013). Regression modeling of the North East Atlantic Spring Bloom suggests previously unrecognized biological roles for V and Mo. *Frontiers in Microbiology*, *4*(March), 1–12. https://doi.org/10.3389/fmicb.2013.00045

Klinkhammer, G. P. (1980). Observations of the distribution of manganese over the east Pacific Rise. *Chemical Geology*, *29*(1–4), 211–226. https://doi.org/10.1016/0009-2541(80)90021-2

Kuss, J., & Kremling, K. (1999). Spatial variability of particle associated trace elements in near-surface waters of the North Atlantic (30°N/60°W to 60°N/2°W), derived by large volume sampling. *Marine Chemistry*, *68*(1–2), 71–86. https://doi.org/10.1016/S0304-4203(99)00066-3

Lam, P. J., & Bishop, J. K. B. (2008). The continental margin is a key source of iron to the HNLC North Pacific Ocean. *Geophysical Research Letters*, *35*(7), 1–5. https://doi.org/10.1029/2008GL033294

Lam, P. J., Bishop, J. K. B., Henning, C. C., Marcus, M. A., Waychunas, G. A., & Fung, I. Y. (2006). Wintertime phytoplankton bloom in the subarctic Pacific supported by continental margin iron. *Global Biogeochemical Cycles*, *20*(1), 1–12. https://doi.org/10.1029/2005GB002557

Lam, P. J., Lee, J. M., Heller, M. I., Mehic, S., Xiang, Y., & Bates, N. R. (2018). Size-fractionated distributions of suspended particle concentration and major phase composition from the U.S. GEOTRACES Eastern Pacific Zonal Transect (GP16). *Marine Chemistry*, *201*(August), 90–107. https://doi.org/10.1016/j.marchem.2017.08.013

Lam, P. J., Ohnemus, D. C., & Auro, M. E. (2015). Size-fractionated major particle composition and concentrations from the US GEOTRACES North Atlantic zonal transect. *Deep-Sea Research Part II Topical Studies in Oceanography*, *116*, 303–320. https://doi.org/10.1016/j.dsr2.2014.11.020

Lam, P. J., Twining, B. S., Jeandel, C., Roychoudhury, A., Resing, J. A., Santschi, P. H., & Anderson, R. F. (2015). Methods for analyzing the concentration and speciation of major and trace elements in marine particles. *Progress in Oceanography*, *133*, 32–42. https://doi.org/10.1016/j.pocean.2015.01.005

Landing, W. M., & Bruland, K. W. (1987). The contrasting biogeochemistry of iron and manganese in the Pacific Ocean. *Geochimica et Cosmochimica Acta*, *51*(1), 29–43. https://doi.org/10.1016/0016-7037(87)90004-4

Lee, J. M., Heller, M. I., & Lam, P. J. (2018). Size distribution of particulate trace elements in the U.S. GEOTRACES Eastern Pacific Zonal Transect (GP16). *Marine Chemistry*, *201*(September), 108–123. https://doi.org/10.1016/j.marchem.2017.09.006

Liao, W.-H., & Ho, T.-Y. (2018). Particulate trace metal composition and sources in the Kuroshio adjacent to the east China sea: The importance of aerosol deposition. *Journal of Geophysical Research: Oceans*, *123*(9), 6207–6223. https://doi.org/10.1029/2018JC014113

Lippiatt, S. M., Brown, M. T., Lohan, M. C., Berger, C. J. M., & Bruland, K. W. (2010). Leachable particulate iron in the Columbia River, estuary, and near-field plume. *Estuarine, Coastal and Shelf Science*, *87*(1), 33–42. https://doi.org/10.1016/j.ecss.2009.12.009

Lippiatt, S. M., Lohan, M. C., & Bruland, K. W. (2010). The distribution of reactive iron in northern Gulf of Alaska coastal waters. *Marine Chemistry*, *121*(1–4), 187–199. https://doi.org/10.1016/j.marchem.2010.04.007

Little, S. H., Archer, C., Milne, A., Schlosser, C., Achterberg, E. P., Lohan, M. C., & Vance, D. (2018). Paired dissolved and particulate phase Cu isotope distributions in the South Atlantic. *Chemical Geology*, *502*(June), 29–43. https://doi.org/10.1016/j.chemgeo.2018.07.022

Little, S. H., Vance, D., Siddall, M., & Gasson, E. (2013). A modeling assessment of the role of reversible scavenging in controlling oceanic dissolved Cu and Zn distributions. *Global Biogeochemical Cycles*, *27*(3), 780–791. https://doi.org/10.1002/gbc.20073

Liu, T., Krisch, S., Hopwood, M. J., Achterberg, E. P., & Mutzberg, A. (2022). Trace metal data from water samples during METEOR cruise M121. PANGAEA. https://doi.org/10.1594/PANGAEA.947275

Luther, G. W., Thibault de Chanvalon, A., Oldham, V. E., Estes, E. R., Tebo, B. M., & Madison, A. S. (2018). Reduction of manganese oxides: Thermodynamic, kinetic and mechanistic considerations for one- versus two-electron transfer steps. *Aquatic Geochemistry*, *24*(4), 257–277. https://doi.org/10.1007/s10498-018-9342-1

Lutjeharms, J. R. E., & Meeuwis, J. M. (1987). The extent and variability of South-East Atlantic upwelling. *South African Journal of Marine Science*, *5*(1), 51–62. https://doi.org/10.2989/025776187784522621

Martin, J. H., Gordon, R. M., Fitzwater, S., & Broenkow, W. W. (1989). Vertex: Phytoplankton/iron studies in the Gulf of Alaska. *Deep-Sea Research, Part A: Oceanographic Research Papers*, *36*(5), 649–680. https://doi.org/10.1016/0198-0149(89)90144-1

Menzel Barraqueta, J.-L., Christian, S., Hélène, P., Arthur, G., Marie, C., Julia, B., et al. (2018). Aluminium in the North Atlantic Ocean and the Labrador Sea (GEOTRACES GA01 section): Roles of continental inputs and biogenic particle removal. https://doi.org/10.5194/bg-2018-39

Menzel Barraqueta, J.-L., Klar, J., Gledhill, M., Schlosser, C., Shelley, R., Planquette, H. F., et al. (2019). Atmospheric deposition fluxes over the Atlantic Ocean: A GEOTRACES case study. *Biogeosciences*, *16*(7), 1525–1542. https://doi.org/10.5194/bg-16-1525-2019

Middag, R., van Hulten, M., van Aken, H. M., Rijkenberg, M. J. A., Gerringa, L. J. A., Laan, P., & de Baar, H. J. (2015). Dissolved aluminium in the ocean conveyor of the West Atlantic Ocean: Effects of the biological cycle, scavenging, sediment resuspension and hydrography. *Marine Chemistry*, *177*, 69–86. https://doi.org/10.1016/j.marchem.2015.02.015

Millero, F. J., Sotolongo, S., & Izaguirre, M. (1987). The oxidation kinetics of Fe(II) in seawater. *Geochimica et Cosmochimica Acta*, *51*(4), 793–801. https://doi.org/10.1016/0016-7037(87)90093-7

Milne, A., Schlosser, C., Wake, B. D., Achterberg, E. P., Chance, R., Baker, A. R., et al. (2017). Particulate phases are key in controlling dissolved iron concentrations in the (sub)tropical North Atlantic. *Geophysical Research Letters*, *44*(5), 2377–2387. https://doi.org/10.1002/2016GL072314

Moffett, J. W., & Ho, J. (1996). Oxidation of cobalt and manganese in seawater via a common microbially catalyzed pathway. *Geochimica et Cosmochimica Acta*, *60*(18), 3415–3424. https://doi.org/10.1016/0016-7037(96)00176-7

Moore, C. M., Mills, M. M., Arrigo, K. R., Berman-Frank, I., Bopp, L., Boyd, P. W., et al. (2013). Processes and patterns of oceanic nutrient limitation. *Nature Geoscience*, *6*(9), 701–710. https://doi.org/10.1038/ngeo1765

Moran, S. B., & Moore, R. M. (1988). Evidence from mesocosm studies for biological removal of dissolved aluminium from sea water. *Nature*, *335*(6192), 706–708. https://doi.org/10.1038/335706a0

Morel, F. M. M., & Price, N. M. (2003). The biogeochemical cycles of trace metals in the oceans. *Science*, *300*(5621), 944–947. https://doi.org/10.1126/science.1083545

Noble, A. E., Lamborg, C. H., Ohnemus, D. C., Lam, P. J., Goepfert, T. J., Measures, C. I., et al. (2012). Basin-scale inputs of cobalt, iron, and manganese from the Benguela-Angola front to the South Atlantic Ocean. *Limnology & Oceanography*, *57*(4), 989–1010. https://doi.org/10.4319/lo.2012.57.4.0989

Noble, A. E., Ohnemus, D. C., Hawco, N. J., Lam, P. J., & Saito, M. A. (2017). Coastal sources, sinks and strong organic complexation of dissolved cobalt within the US North Atlantic GEOTRACES transect GA03. *Biogeosciences*, *14*(11), 2715–2739. https://doi.org/10.5194/bg-14-2715-2017

Nozaki, Y., Thomson, J., & Turekian, K. K. (1976). The distribution of 210Pb and 210Po in the surface waters of the Pacific Ocean. *Earth and Planetary Science Letters*, *32*(2), 304–312. https://doi.org/10.1016/0012-821X(76)90070-4

Nuester, J., Vogt, S., Newville, M., Kustka, A. B., & Twining, B. S. (2012). The unique biogeochemical signature of the marine diazotroph trichodesmium. *Frontiers in Microbiology*, *3*(April), 150. https://doi.org/10.3389/FMICB.2012.00150

Ohnemus, D. C., & Lam, P. J. (2015). Cycling of lithogenic marine particles in the US GEOTRACES North Atlantic transect. *Deep-Sea Research Part II Topical Studies in Oceanography*, *116*, 283–302. https://doi.org/10.1016/j.dsr2.2014.11.019

Ohnemus, D. C., Lam, P. J., & Twining, B. S. (2018). Optical observation of particles and responses to particle composition in the GEOTRACES GP16 section. *Marine Chemistry*, *201*, 124–136. https://doi.org/10.1016/J.MARCHEM.2017.09.004

Ohnemus, D. C., Rauschenberg, S., Cutter, G. A., Fitzsimmons, J. N., Sherrell, R. M., & Twining, B. S. (2017). Elevated trace metal content of prokaryotic communities associated with marine oxygen deficient zones. *Limnology & Oceanography*, *62*(1), 3–25. https://doi.org/10.1002/LNO.10363

Orians, K. J., & Bruland, K. W. (1986). The biogeochemistry of aluminum in the Pacific Ocean. *Earth and Planetary Science Letters*, *78*(4), 397–410. https://doi.org/10.1016/0012-821x(86)90006-3

Origin(Pro). (2021). *Version (9.80)*. OriginLab Corporation.

Peterson, R. G., & Stramma, L. (1991). Upper-level circulation in the south Atlantic Ocean. *Progress in Oceanography*, *26*(1), 1–73. https://doi.org/10.1016/0079-6611(91)90006-8

Porto, F. G. M., Neto, M. C. A., & Finzer, J. R. D. (2018). Solubility of phosphate rocks in citric acid. *World Scientific Research*, *5*(1), 32–36. https://doi.org/10.20448/journal.510.2018.51.32.36

Prasad, M. S. (1989). Production of copper and cobalt at Gecamines, Zaire. *Minerals Engineering*, *2*(4), 521–541. https://doi.org/10.1016/0892-6875(89)90087-3

Prospero, J. M. (1996). Saharan dust transport over the North Atlantic Ocean and Mediterranean: An overview (pp. 133–151). https://doi.org/10.1007/978-94-017-3354-0_13

Rahlf, P. (2020). Tracing water masses and terrestrial inputs with radiogenic neodymium and hafnium isotopes and rare earth elements in the southeastern Atlantic Ocean (thesis). Retrieved from https://macau.uni-kiel.de/receive/macau_mods_00001033?lang=de

Rahlf, P., Hathorne, E., Laukert, G., Gutjahr, M., Weldeab, S., & Frank, M. (2020). Tracing water mass mixing and continental inputs in the southeastern Atlantic Ocean with dissolved neodymium isotopes. *Earth and Planetary Science Letters*, *530*, 115944. https://doi.org/10.1016/J.EPSL.2019.115944

Rahlf, P., Laukert, G., Hathorne, E. C., Vieira, L. H., & Frank, M. (2021). Dissolved neodymium and hafnium isotopes and rare Earth elements in the Congo River Plume: Tracing and quantifying continental inputs into the southeast Atlantic. *Geochimica et Cosmochimica Acta*, *294*, 192–214. https://doi.org/10.1016/J.GCA.2020.11.017

Raiswell, R., & Canfield, D. E. (2012). The iron biogeochemical cycle past and present. *Geochemical Perspectives*, *1*(1), 1–232. https://doi.org/10.7185/geochempersp.1.1

Rapp, I., Schlosser, C., Menzel Barraqueta, J.-L., Wenzel, B., Lüdke, J., Scholten, J., et al. (2019). Controls on redox-sensitive trace metals in the Mauritanian oxygen minimum zone. *Biogeosciences*, *16*(21), 4157–4182. https://doi.org/10.5194/bg-16-4157-2019

Rapp, I., Schlosser, C., Rusiecka, D., Gledhill, M., & Achterberg, E. P. (2017). Automated preconcentration of Fe, Zn, Cu, Ni, Cd, Pb, Co, and Mn in seawater with analysis using high-resolution sector field inductively-coupled plasma mass spectrometry. *Analytica Chimica Acta*, *976*, 1–13. https://doi.org/10.1016/j.aca.2017.05.008

Rauschenberg, S., & Twining, B. S. (2015). Evaluation of approaches to estimate biogenic particulate trace metals in the ocean. *Marine Chemistry*, *171*, 67–77. https://doi.org/10.1016/j.marchem.2015.01.004

Richon, C., & Tagliabue, A. (2019). Insights into the major processes driving the global distribution of copper in the ocean from a global model. *Global Biogeochemical Cycles*, *33*(12), 1594–1610. https://doi.org/10.1029/2019GB006280

Rudnick, R. L., & Gao, S. (2013). Composition of the continental crust. In *Treatise on geochemistry*, 2nd ed. (Vol. 4). Elsevier Ltd. https://doi.org/10.1016/B978-0-08-095975-7.00301-6

Rue, E. L., & Bruland, K. W. (1995). Complexation of iron(III) by natural organic ligands in the Central North Pacific as determined by a new competitive ligand equilibration/adsorptive cathodic stripping voltammetric method. *Marine Chemistry*, *50*(1–4), 117–138. https://doi.org/10.1016/0304-4203(95)00031-L

Rusiecka, D., Gledhill, M., Milne, A., Achterberg, E. P., Annett, A. L., Atkinson, S., et al. (2018). Anthropogenic signatures of lead in the Northeast Atlantic. *Geophysical Research Letters*, *45*(6), 2734–2743. https://doi.org/10.1002/2017GL076825

Rutgers Van Der Loeff, M. M., & Boudreau, B. P. (1997). The effect of resuspension on chemical exchanges at the sediment-water interface in the deep sea—A modelling and natural radiotracer approach. *Journal of Marine Systems*, *11*(3–4), 305–342. https://doi.org/10.1016/S0924-7963(96)00128-5

Schlitzer, R. (2018). Ocean data view. Retrieved from https://odv.awi.de

Schlosser, C., & Garbe-Schönberg, D. (2019). Mechanisms of Pb supply and removal in two remote (sub-)polar ocean regions. *Marine Pollution Bulletin*, *149*, 110659. https://doi.org/10.1016/J.MARPOLBUL.2019.110659

Schlosser, C., Streu, P., Frank, M., Lavik, G., Croot, P. L., Dengler, M., & Achterberg, E. P. (2018). H2S events in the Peruvian oxygen minimum zone facilitate enhanced dissolved Fe concentrations. *Scientific Reports*, *8*(1), 12642. https://doi.org/10.1038/s41598-018-30580-w

Scholz, F., Löscher, C. R., Fiskal, A., Sommer, S., Hensen, C., Lomnitz, U., et al. (2016). Nitrate-dependent iron oxidation limits iron transport in anoxic ocean regions. *Earth and Planetary Science Letters*, *454*, 272–281. https://doi.org/10.1016/j.epsl.2016.09.025

Shannon, L. V. (2001). Benguela current. In *Encyclopedia of ocean sciences* (1st ed., pp. 225–267).

Shannon, L. V., Agenbag, J. J., & Buys, M. E. L. (1987). Large- and mesoscale features of the Angola-Benguela front. *South African Journal of Marine Science*, *5*(1), 11–34. https://doi.org/10.2989/025776187784522261

Shannon, L. V., & Nelson, G. (1996). The Benguela: Large scale features and processes and system variability. *The South Atlantic*, 163–210. https://doi.org/10.1007/978-3-642-80353-6_9

Sherrell, R. M., & Boyle, E. A. (1992). The trace metal composition of suspended particles in the oceanic water column near Bermuda. *Earth and Planetary Science Letters*, *111*(1), 155–174. https://doi.org/10.1016/0012-821x(92)90176-v

Sunda, W. G. (1989). Trace metal interactions with marine phytoplankton. *Biological Oceanography*, *6*, 411–442. https://doi.org/10.1080/01965581.1988.10749543

Sunda, W. G. (2012). Feedback interactions between trace metal nutrients and phytoplankton in the ocean. *Frontiers in Microbiology*, *3*(June), 1–22. https://doi.org/10.3389/fmicb.2012.00204

Sunda, W. G., & Huntsman, S. A. (1988). Effect of sunlight on redox cycles of manganese in the southwestern Sargasso Sea. *Deep-Sea Research, Part A: Oceanographic Research Papers*, *35*(8), 1297–1317. https://doi.org/10.1016/0198-0149(88)90084-2

Sunda, W. G., & Huntsman, S. A. (1994). Photoreduction of manganese oxides in seawater. *Marine Chemistry*, *46*(1–2), 133–152. https://doi.org/10.1016/0304-4203(94)90051-5

Taylor, S. R., & McLennan, S. M. (1995). The geochemical evolution of the continental crust. *Reviews of Geophysics*, *33*(2), 241–265. https://doi.org/10.1029/95RG00262

Tebo, B. M., Bargar, J. R., Clement, B. G., Dick, G. J., Murray, K. J., Parker, D., et al. (2004). Biogenic manganese oxides: Properties and mechanisms of formation. *Annual Review of Earth and Planetary Sciences*, *32*(1954), 287–328. https://doi.org/10.1146/annurev.earth.32.101802.120213

Tebo, B. M., Johnson, H. A., McCarthy, J. K., & Templeton, A. S. (2005). Geomicrobiology of manganese(II) oxidation. *Trends in Microbiology*, *13*(9), 421–428. https://doi.org/10.1016/j.tim.2005.07.009

Tovar-Sanchez, A., Sañudo-Wilhelmy, S. A., Kustka, A. B., Agustí, S., Dachs, J., Hutchins, D. A., et al. (2006). Effects of dust deposition and river discharges on trace metal composition of *Trichodesmium* spp. in the tropical and subtropical North Atlantic Ocean. *Limnology & Oceanography*, *51*(4), 1755–1761. https://doi.org/10.4319/LO.2006.51.4.1755

Turekian, K. K. (1977). The fate of metals in the oceans. *Geochimica et Cosmochimica Acta*, *41*(8), 1139–1144. https://doi.org/10.1016/0016-7037(77)90109-0

Twining, B. S., & Baines, S. B. (2013). The trace metal composition of marine phytoplankton. *Annual Review of Marine Science*, *5*(1), 191–215. https://doi.org/10.1146/annurev-marine-121211-172322

Twining, B. S., Baines, S. B., Bozard, J. B., Vogt, S., Walker, E. A., & Nelson, D. M. (2011). Metal quotas of plankton in the equatorial Pacific Ocean. *Deep-Sea Research Part II Topical Studies in Oceanography*, *58*(3–4), 325–341. https://doi.org/10.1016/j.dsr2.2010.08.018

Twining, B. S., Nodder, S. D., King, A. L., Hutchins, D. A., LeCleir, G. R., DeBruyn, J. M., et al. (2014). Differential remineralization of major and trace elements in sinking diatoms. *Limnology and Oceanography*, *59*(3), 689–704. https://doi.org/10.4319/lo.2014.59.3.0689

Twining, B. S., Rauschenberg, S., Baer, S. E., Lomas, M. W., Martiny, A. C., & Antipova, O. (2019). A nutrient limitation mosaic in the eastern tropical Indian Ocean. *Deep-Sea Research Part II Topical Studies in Oceanography*, *166*, 125–140. https://doi.org/10.1016/j.dsr2.2019.05.001

Twining, B. S., Rauschenberg, S., Morton, P. L., & Vogt, S. (2015). Metal contents of phytoplankton and labile particulate material in the North Atlantic Ocean. *Progress in Oceanography*, *137*, 261–283. https://doi.org/10.1016/j.pocean.2015.07.001

van den Berg, C. M. G. (1995). Evidence for organic complexation of iron in seawater. *Marine Chemistry*, *50*(1–4), 139–157. https://doi.org/10.1016/0304-4203(95)00032-M

van der Merwe, P., Bowie, A. R., Quéroué, F., Armand, L., Blain, S., Chever, F., et al. (2015). Sourcing the iron in the naturally fertilised bloom around the Kerguelen Plateau: Particulate trace metal dynamics. *Biogeosciences*, *12*(3), 739–755. https://doi.org/10.5194/bg-12-739-2015

van der Merwe, P., Wuttig, K., Holmes, T. M., Trull, T. W., Chase, Z., Townsend, A. T., et al. (2019). High lability Fe particles sourced from glacial erosion can meet previously unaccounted biological demand: Heard Island, Southern Ocean. *Frontiers in Marine Science*, *6*(June), 1–20. https://doi.org/10.3389/fmars.2019.00332

Vangriesheim, A., Pierre, C., Aminot, A., Metzl, N., Baurand, F., & Caprais, J. C. (2009). The influence of Congo River discharges in the surface and deep layers of the Gulf of Guinea. *Deep-Sea Research Part II Topical Studies in Oceanography*, *56*(23), 2183–2196. https://doi.org/10.1016/j.dsr2.2009.04.002

Vedamati, J., Chan, C., & Moffett, J. W. (2015). Distribution of dissolved manganese in the Peruvian upwelling and oxygen minimum zone. *Geochimica et Cosmochimica Acta*, *156*, 222–240. https://doi.org/10.1016/j.gca.2014.10.026

Vieira, L. H., Krisch, S., Hopwood, M. J., Beck, A. J., Scholten, J., Liebetrau, V., & Achterberg, E. P. (2020). Unprecedented Fe delivery from the Congo River margin to the South Atlantic Gyre. *Nature Communications*, *11*(1), 1–8. https://doi.org/10.1038/s41467-019-14255-2

von Langen, P. J., Johnson, K. S., Coale, K. H., & Elrod, V. A. (1997). Oxidation kinetics of manganese (II) in sea water at nanomolar concentrations. *Geochimica et Cosmochimica Acta*, *61*(23), 4945–4954. https://doi.org/10.1016/S0016-7037(97)00355-4

Weber, T. S., & Bianchi, D. (2020). Efficient particle transfer to depth in oxygen minimum zones of the Pacific and Indian oceans. *Frontiers of Earth Science*, *8*(September), 1–11. https://doi.org/10.3389/feart.2020.00376

Weber, T. S., John, S., Tagliabue, A., & DeVries, T. (2018). Biological uptake and reversible scavenging of zinc in the global ocean. *Science*, *361*(6397), 72–76. https://doi.org/10.1126/science.aap8532

Wells, M. L., Price, N. M., & Bruland, K. W. (1995). Iron chemistry in seawater and its relationship to phytoplankton: A workshop report. *Marine Chemistry*, *48*(2), 157–182. https://doi.org/10.1016/0304-4203(94)00055-i

Winkler, L. W. (1888). The determination of dissolved oxygen in water. *Berlin DeutChem Gas*, *21*, 2843–2855. Retrieved from https://ci.nii.ac.jp/naid/20001681874

Wuttig, K., Townsend, A. T., van der Merwe, P., Gault-Ringold, M., Holmes, T., Schallenberg, C., et al. (2019). Critical evaluation of a seaFAST system for the analysis of trace metals in marine samples. *Talanta*, *197*(November), 653–668. https://doi.org/10.1016/j.talanta.2019.01.047

Xiang, Y., & Lam, P. J. (2020). Size-Fractionated compositions of marine suspended particles in the Western Arctic Ocean: Lateral and vertical sources. *Journal of Geophysical Research: Oceans*, *125*(8), 1–33. https://doi.org/10.1029/2020JC016144

Yang, W., Guo, L., Chuang, C. Y., Santschi, P. H., Schumann, D., & Ayranov, M. (2015). Influence of organic matter on the adsorption of 210Pb, 210Po and 7Be and their fractionation on nanoparticles in seawater. *Earth and Planetary Science Letters*, *423*, 193–201. https://doi.org/10.1016/j.epsl.2015.05.007

Zheng, L., Minami, T., Takano, S., Ho, T.-Y., & Sohrin, Y. (2021). Sectional distribution patterns of Cd, Ni, Zn, and Cu in the North Pacific ocean: Relationships to Nutrients and importance of scavenging. *Global Biogeochemical Cycles*, *35*(7), e2020GB006558. https://doi.org/10.1029/2020GB006558

## References From the Supporting Information

Jochum, K. P., Nohl, U., Herwig, K., Lammel, E., Stoll, B., & Hofmann, A. W. (2005). GeoReM: A new geochemical database for reference materials and isotopic standards. *Geostandards and Geoanalytical Research*, *29*(3), 333–338. https://doi.org/10.1111/j.1751-908x.2005.tb00904.x